CHEMICAL IONIZATION AND ION MOLECULE REACTIONS IN THE QUADRUPOLE ION TRAP MASS SPECTROMETER WITH ION INJECTION

By

GEORGE BRODY GUCKENBERGER, V

A DISSERTATION PRESENTED TO THE GRADUATE SCHOOL
OF THE UNIVERSITY OF FLORIDA IN PARTIAL FULFILLMENT
OF THE REQUIREMENTS FOR THE DEGREE OF
DOCTOR OF PHILOSOPHY

UNIVERSITY OF FLORIDA

1999

To You

ACKNOWLEDGMENTS

I wish to express my thanks to Dr. Richard A. Yost for his guidance in the completion of this work and for keeping his door open the past few years. I also wish to thank the members of my graduate committee, Drs. Christopher D. Batich, John R. Eyler, Luis M. Muga, and William Weltner. I would like to thank current members of the Yost group, James Murphy, Joseph McClellan, Kevin Joseph McHale, Joseph Mulholland, and Rick Joseph Troendle (I had to accentuate the similarities in their names) for interesting lunch conversations and for putting up with me for an extra year. I especially want to thank past Yosties, Dr. Jodie Johnson, Dr. Stephen Boue (my surfing pal), and Dr. Scott Quarmby for their friendship and for always stopping to express interest in what I was doing. Special thanks to Scott and Steve for finding all the parts for and putting together SweetP's table and vacuum control. Scott brought the octapole and vacuum chamber for SweetP back with him from a summer at Finnigan, and put the first build of the instrument together with the TSQ source and ITS-40 trap.

I would like to acknowledge and thank Finnigan (George Stafford and Eric Johnson in particular) for supporting my research and giving me the wonderful opportunity to work at Finnigan in Austin, Texas, for two summers.

Special thanks belong to Dr. Lynmarie A. Posey for giving me a start in research at Vanderbilt University and encouraging me to go to graduate school.

I am indebted to David Gonzalez for giving me ideas for chiral compounds and making the acetonides for my Diels-Alder reactions.

I would like to acknowledge my lovely wife Alison for her hand in getting me to Florida, for her support throughout my graduate career, and for giving me the inspiration to finish this dissertation.

Finally, I would like to thank God for his spiritual guidance and bestowing his grace upon me so that I might complete this work.

TABLE OF CONTENTS

page

ACKNOWLEDGMENTS iii

ABSTRACT vii

CHAPTERS

1 INTRODUCTION 1

The Quadrupole Ion Trap Mass Spectrometer 2
General Operation 2
Ion Injection 5
Ionization 6
Electron Ionization 6
Chemical Ionization 8
Ion/Molecule Reactions in the Quadrupole Ion Trap 10
Overview of Dissertation 12

2 INSTRUMENTATION FOR ION INJECTION 14

General Overview 14
Instrument Design 15
Commercial QITMS: Finnigan GCQ 15
Differentially Pumped QITMS: SweetP 21
Characterization of GCQ and SweetP Instrument Parameters 25
Injection RF Level 25
Ion Optics 29
Helium Buffer Gas 31
Resonant Excitation Voltage 34
Tuning the GCQ Electronics for CI 37
Optimization of CI Parameters 39
Calculating Reaction Time 49
Calculation of Number of Ions in the QITMS 51
Conclusions 51

3 CHIRAL ION/MOLECULE REACTIONS 53

General Overview 53
Diels-Alder Ion/Molecule Reactions 54
Background 54
Choosing Chiral Reactants 56
Experimental 59
Results 62
Conclusions 64
Isopinocampheol Reactions with Phenylethylamine 64
Experimental 65
Results 67
Conclusions 75

4 ION/MOLECULE REACTIONS WITH WATER 77

Introduction 77
Argon and Water Sensitivity on the RGA 82
Water in the QITMS from Trapping Helium 85
Air/Water Spectra 86
Trimethylsilyl Derivatives of Organic Acids 93
Experimental 93
TMS Derivative Spectra 94
Use as a Hygrometer 99
Conclusions 106

5 CONCLUSIONS AND FUTURE WORK 108

GLOSSARY 113

LIST OF REFERENCES 115

BIOGRAPHICAL SKETCH 118

Abstract of Dissertation Presented to the Graduate School
of the University of Florida in Partial Fulfillment of the
Requirements for the Degree of Doctor of Philosophy

CHEMICAL IONIZATION AND ION MOLECULE REACTIONS
IN THE QUADRUPOLE ION TRAP MASS SPECTROMETER
WITH ION INJECTION

By

George Brody Guckenberger, V

May 1999

Chairman: Richard A. Yost
Major Department: Chemistry

This dissertation presents research conducted on two quadrupole ion trap mass spectrometers (QITMS), each with ion injection (spatial separation of the ion source from the ion trap). Experiments used to develop and characterize the ion injection QITMS instrumentation are discussed as well as those used to demonstrate the utility of the instrumentation for the study of gas-phase ion/molecule reactions within the QITMS.

In characterization of the ion source and in preparation for ion/molecule reaction studies within the QITMS, chemical ionization parameters were optimized. Injection energies, reagent gas pressure in the ion source and trapping gas pressure were among the parameters that had to be characterized to be able to efficiently produce and trap ions.

Ion/molecule studies were conducted on the QITMS to show the advantages of ion injection for selecting specific chemical reactions for study without interference from

neutral species from the ion source. Diels-Alder cycloaddition reactions and condensation reactions between chiral reactant ions and neutrals were studied to see if the selectivity of the reactions in the QITMS could enhance differences in the reactions between different enantiomers. Differences in collision-induced dissociation spectra of the reaction products were also studied for chiral differentiation.

Ion/molecule reactions between ions of trimethylsilyl derivatives of organic acids and neutral water vapor were studied to see the effects of water reactions in QITMS spectra. The kinetics of these reactions were found to be first order with respect to water concentration and first order with respect to ion concentration. The use of these reactions as a hygrometer for the QITMS is suggested.

CHAPTER 1
INTRODUCTION

This dissertation discusses research conducted on two quadrupole ion trap mass spectrometers (QITMS), each with ion injection (the ability to generate ions in an external source and then to guide these ions into the ion trap). The goals of the research were twofold: first, to develop and characterize ion injection QITMS instrumentation with broad ranging application utility, and second, to demonstrate the utility of the instrumentation for the study of gas-phase ion/molecule reactions. In characterization of the ion source and preparation for ion/molecule reaction studies within the QITMS, several ionization techniques were investigated in the external source for ion injection. These techniques included chemical ionization (CI), electron ionization (EI), matrix-assisted laser desorption ionization (MALDI), and laser desorption chemical ionization (LDCI). Among these, chemical ionization required the greatest study and optimization for use with the ion trap. It has not previously been well characterized with ion injection into the QITMS. Injection energies, reagent gas pressure in the ion source and trapping gas pressure were among the parameters that had to be evaluated to be able to efficiently produce and trap ions. Ion/molecule studies were conducted on the QITMS to show the advantages of ion injection for selecting specific chemical reactions for study without interference from neutral species from the ion source. The hope was that some chiral ion/molecule reactions could be investigated taking advantage of the tandem mass

spectrometry (MS/MS or MS^n) capabilities of the QITMS in such a fashion as to amplify any chiral selectivity these reactions may exhibit.

This chapter will give a brief introduction to the quadrupole ion trap, introduce the ionization techniques investigated in the external source, and present some background for study of ion/molecule reactions in the gas phase as they pertain to this work. This chapter then concludes with an overview of the dissertation.

The Quadrupole Ion Trap Mass Spectrometer

General Operation

While the theory of the ion trap is necessary for the development and use of the ion trap, it can be quite unwieldy in textual form. It is not necessary to describe in detail how the ion trap functions to understand this work. This text will serve to review the general operation of the now widely-used QITMS and forgo the ion trap theory found in most other ion trap dissertations. For a good mathematical description of ion trap theory consult March and Londry (1995).

The quadrupole ion trap (QIT) is composed of three radially symmetric hyperbolic electrodes. Figure 1-1 depicts a cross section of these electrodes (two endcap electrodes and one ring electrode). A radiofrequency (RF) voltage is applied to the ring electrode at variable amplitudes and fixed frequency, causing ions injected into the trap to oscillate and remain trapped inside. An ion's frequency of motion in the trap is defined by its mass-to-charge ratio (m/z) at a specific RF amplitude (IonRf). Ions of higher m/z will have lower frequency of motion compared to ions of lower m/z. The m/z range of ions able to be held stable within the ion trap is determined by the IonRf. IonRf is

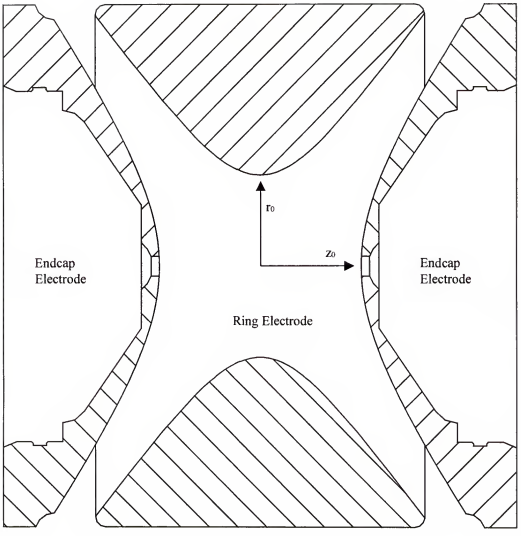

Figure 1-1: Drawing of the QITMS. The electrodes are radially symmetric about the z-axis. Ions enter and exit through the holes in the endcap electrodes.

typically expressed in units of m/z for practical use. For example, when the IonRf is set to m/z 30, ions with a mass-to-charge ratio less than or equal to m/z 30 will be unstable and ejected from the ion trap. Ions with a mass-to-charge ratio greater than m/z 30 will be stable in the ion trap. Because ions of different m/z may have different internal and kinetic energies upon ion injection, the IonRf may be varied to optimize trapping efficiency. This will be discussed briefly in Chapter 2.

Mass analysis in the QITMS is performed by raising the IonRf and sequentially ejecting ions of increasing m/z. Resolution is improved by adding a supplementary AC or resonant ejection voltage across the endcap electrodes at the frequency of the ions just prior to normal ejection from the trap due to IonRf instability (Stafford et al., 1985). For mass analysis, the resonant ejection amplitude is calibrated to eject ions of different m/z with the best possible resolution. Ions of low m/z are observed to require less amplitude than high m/z ions to be effectively ejected from the QITMS.

The QITMS has the ability to perform sequential stages of mass spectrometry in which a specific m/z or range of m/z is isolated in the trap, dissociated, chemically reacted, or otherwise perturbed, and then the product ions are studied by another stage of mass analysis. By sequential stages of ion isolation and mass analysis, ion traps have the ability to perform what is termed MS/MS or MS^n (Johnson et al., 1990).

Normal operation of the QITMS for MS/MS involves applying resonant excitation waveforms to the QIT at variable frequencies to eject all unwanted ions and isolate the m/z or m/z range of interest. The resonant excitation voltage is then applied to the isolated ions at an amplitude sufficient to raise the kinetic energy of the ions to undergo collisions with a neutral collision gas and dissociate to form fragment ions (collision-induced dissociation, CID). The collision gas is most often helium at a pressure of approximately 1 mTorr, which is used as a buffer gas to aid in the damping and trapping of ions in the QIT. Maximum ion internal energies resulting from resonantly excited collisions typically range from 2 to 4 eV (Basic et al., 1994; Johnson et al. 1995). For ion/molecule reactions, resonant excitation is not used, and the ions are

held in the trap and allowed to react with neutrals in the trap before the next stage of mass spectrometry.

Ion Injection

Commercial versions of the QITMS were initially designed for internal ionization. Ions were generated within the ion trap by gating electrons into the trap, which ionized the analyte in electron ionization (EI) or a reagent gas for chemical ionization (CI) of the analyte. The ion trap was very sensitive with internal ionization; however, it was limited in ionization methods available and had disadvantages for studying selective ion/molecule reactions. For example, the analyte was added directly into the ion trap, so that analyte neutrals could react with analyte ions to form unwanted adduct ions or undergo competing ion/molecule reactions (Coopersmith, 1994).

By spatial separation of the ion source from the QIT, ion injection offers several advantages over internal ionization (Yost and Pedder, 1989). First, the restrictions of low-pressure gas-phase ionization are lifted, allowing for high-pressure ionization techniques such as CI or electrospray. Second, the sample matrix is separate from the ion-trapping region, reducing problems with ion/molecule reactions. Third, the number and mass range of ions admitted into the trap can be controlled, reducing ion-ion space charge, which can cause problems with sensitivity, mass accuracy, and resolution. Fourth, the polarity of ions injected into the trap is controlled, eliminating problems with ion-ion recombination reactions. Finally, the source is more accessible when separated from the ion trap and its controlling electronics.

Ion injection has some disadvantages. Losses in sensitivity occur due to poor ion transmission through ion optics from the source. Injection into the ion trap is not wholly efficient either. Ion injection efficiency exhibits a dependence upon the RF phase during injection (Moore and Gulick, 1987; Quarmby, 1997). Ion injection also exhibits some mass discrimination due to the IonRf during injection. Finally, ions accelerated from the source into the QIT should be cooled by collisions with a buffer gas to help confine them in the trap. The loss of momentum due to collisions with the buffer gas helps reduce ion kinetic energy to a level less than the potential well depth of the QIT appropriate to the trapping conditions (March and Hughes, 1989). Unfortunately, these collisions may add to the ion internal energy and cause fragmentation.

Ionization

The instruments used for ion injection and ion/molecule studies were capable of producing ions by several ionization techniques. The following sections describe the basic premises of two of these ionization methods used most, EI and CI.

Electron Ionization

In EI, electrons are emitted from a rhenium filament and spiral under the influence of source magnets through the ion source region (the ion volume) towards a grounded surface. While passing through the ion volume, they interact with molecules to create ions. In positive EI, the interaction between an electron and an analyte molecule has an efficiency of about 1 in 1000 to produce an ion (Chapman, 1985). Positive ion formation occurs primarily by the following process: $e^- + M \rightarrow M^{+\cdot} + 2e^-$ (1-1)

The electron kinetic energy is typically set between 50 to 100 eV for positive EI. The electron energy is defined by the potential difference between the filament and the source ground. Because the ionization energies of most organic species are on the order of 10 eV, the molecular radical ions often have excess energy from the interaction with the higher energy electron and typically dissociate to fragment ions. In negative EI, ions are formed according to the following processes (Rankin, 1971):

Resonance capture: $AB + e^- \rightarrow AB^-$ (1-2)

Dissociative resonance capture: $AB + e^- \rightarrow A^- + B$ (1-3)

Ion pair formation: $AB + e^- \rightarrow A^- + B^+ + e^-$ (1-4)

Resonance capture or electron capture occurs when the electron energy is less than 2 eV. The term resonance is used to denote that excess energy is distributed throughout the ion rather than being carried away by emitting an electron (Harris, 1992). Electrons responsible for electron capture are either emitted from the filament at a higher energy and thermalized by inelastic collisions with a buffer gas in the source (Warman and Sauer, 1975; Harris, 1992), or are secondary electrons from fragmentation of other molecules in the source (Rankin, 1971). The filament cannot efficiently emit such low energy electrons into the source. Molecular anion production in electron capture is improved as buffer molecules in the source more efficiently thermalize low-energy electrons and collisionally stabilize excited molecular anions (Sears and Grimsrud, 1989). Electron capture is therefore often referred to as negative CI due to its reliance on a buffer gas. Dissociative resonance capture occurs for electron energies of 2 to 10 eV, whereas, ion pair formation occurs when the electron energy is on the order of 10 eV or more.

Negative EI can be as much as 10,000 times less sensitive than positive EI (Rankin, 1971; Chapman, 1985).

Chemical Ionization

Chemical ionization generally describes a vast array of ionization techniques involving ion/molecule reactions between a reagent ion, or series of reagent ions, and the analyte. The reagent ions may be formed from a number of different gases, molecules, or even analyte molecules, which readily react with the species under study. Several reagents were investigated in this study for efficient production of ions used in the ion/molecule reactions and charactization of the instrumentation. These included ammonia, carbon dioxide, isobutane, methane, and phenylethylamine. These reagents will not be individually discussed unless specifically involved in the reactions mentioned in the following chapters. Harrison (1992) offers a comprehensive review of the reactions involved in CI. This text will serve to briefly explain these basic reactions that occur in CI.

In positive CI the following ion/molecule reactions predominate:

Charge exchange: $X^{+\cdot} + M \rightarrow M^{+\cdot} + X$ (1-5)

Quite often in charge exchange, the recombination energy of the reactant ion, $X^{+\cdot}$, is greater than the ionization energy of the neutral, M, and the exothermicity of the reaction causes further fragmentation of the $M^{+\cdot}$ product ion.

Proton transfer: $XH^{+} + M \rightarrow MH^{+} + X$ (1-6)

Endothermic proton transfer reactions are not favorable; however, if the proton affinity of the neutral M is greater than the reagent X, the reaction is favorable. If both species have

similar proton affinities, the ionization is often gentle enough to produce a stable MH^+ ion. It is very common for this reaction to occur with an ion and molecule of the same species. In this case, we have a self-CI reaction (1-7).

Self-protonation: $M^{+\cdot} + M \rightarrow MH^+ + [M - H]^{\cdot}$ (1-7)

Hydride abstraction: $X^+ + M \rightarrow [M - H]^+ + XH$ (1-8)

Condensation: $A^+ + B \rightarrow [AB^+]^* \rightarrow AB^+ \rightarrow C^+ + D$ (1-9)

Association: $A^+ + B \rightarrow AB^+$ (1-10)

Association and condensation reactions are very similar in that they both can form an adduct ion, AB^+, which can be collisionally stabilized and observed. The difference between them is that if the adduct ion is not stabilized, the condensation complex fragments to form new products, while the association complex dissociates to reform the reactants (Harrison, 1992). These two reactions will be discussed with the ion/molecule reactions in Chapter 3 and again in Chapter 4 with the discussion of water reactions.

In addition to electron capture (1-2) mentioned above, the following reactions are seen in negative CI:

Displacement: $X^- + RY \rightarrow RX + Y^-$ (1-11)

Elimination: $X^- + RY \rightarrow [X+H] + [R - H] + Y^-$ (1-12)

The elimination reaction is common among oxyanions and alkyl halides (Depuy et al.,1990).

Proton transfer: $X^- + YH \rightarrow XH + Y^-$ (1-13)

Charge exchange: $X^{-\cdot} + Y \rightarrow Y^{-\cdot} + X$ (1-14)

Association: $X^- + Y \rightarrow XY^-$ (1-15)

Negative CI can be much more sensitive than EI or positive CI for those compounds that have high electron affinity (Harrison, 1992). For example, on the commercial GC/MS instrument used in this work, 0.1 picogram of decafluorobenzophenone produces a mass peak in electron capture negative CI with equivalent signal-to-noise as the mass peak acquired for 100 times more sample (10 picograms) in positive EI.

In addition to simple gas-phase CI in which the sample is introduced into the source via capillary GC, direct exposure or solids probe, laser desorption CI was also investigated as a means of producing ions from involatile samples. Analyte was desorbed from a sample within a standard CI ion volume by a pulse from a nitrogen laser. The desorbed sample was then ionized by EI and/or CI. This work is currently under investigation in our lab by Rick Troendle and will receive some brief mention in the next chapter's discussion on instrumentation.

Ion/Molecule Reactions in the Quadrupole Ion Trap

Mass spectrometry has a rich history of providing useful information in gas-phase chemistry. The number of papers written concerning ion energetics as well as gas-phase thermodynamic and kinetic data is overwhelming. This dissertation cannot comprehensively review the vast field of ion/molecule chemistry that has been previously explored. This dissertation will focus on the selectivity of the QITMS for ion/molecule research.

Selective ion/molecule reactions taking advantage of the MS/MS capabilities of the QITMS have been previously studied in our laboratory (Berberich, 1989;

Coopersmith, 1994). The instrumentation described in this dissertation takes advantage of the MS/MS selectivity of the QITMS for isolating specific ions for gas-phase study and adds the selectivity of ion injection for spatially isolating the reaction vessel from the ion source. The focus of the ion/molecule research for this dissertation has been to study reactions either for the purpose of characterizing the instrument (water reactions) or for the purpose of discovering reactions that might yield structural information in the analysis of isomeric species, specifically enantiomers. In the search for reactions that might offer some form of chiral selectivity, the reaction should ideally form a product that sterically favors one reaction over another. Diels-Alder ion/molecule reactions form cyclic products that should be able to lock in the stereochemistry of the reactants into the product ion rather than allow rearrangement to non-distinctive products. Diels–Alder reactions have been reported to occur in ion/molecule chemistry within the QITMS (Lu et al., 1995; Soni et al., 1995). Differences in gas-phase reactivities due to steric hindrances may even be possible. Sellier et al. (1994) reported enantioselectivity in both CI product ion formation and MS/MS of products using chiral CI reagent gases. These reactions will be discussed in Chapter 3.

Ion/molecule reactions in the QITMS have previously been referred to as both a nuisance and an advantage. The advantages of ion/molecule reactions for both structure elucidation of isomeric species (Splitter and Turecek (1994) offer an excellent review) and for the study of gas-phase chemistry such as gas-phase basicities, acidities, and reaction kinetics are well recognized (Brodbelt, 1995). This dissertation discusses ion/molecule reactions involved in structure elucidation of enantiomeric species in an attempt to take advantage of the positive aspects of ion-neutral chemistry. On the

negative side, however, reactions considered a nuisance, such as water reactions that are not eliminated by displacing the ion source from the QIT, are also investigated to determine the effects on spectral quality and reproducibility.

Mass spectra from ion traps often include interesting peaks not seen in spectra from quadrupole or sector instruments. There are questions as to whether some of these strange ions are the result of ion/molecule reactions occurring within the ion trap as a result of long residence times with neutrals present, or are the result of other processes within the QITMS. Some studies were performed in the ion injection instruments to answer spectral questions concerning whether the production of various unusual ions in QITMS EI and CI spectra occurred in the ion source or in the ion trap. For example, by varying ion injection energies during the injection of methyl stearate ions, studies with this instrumentation were able to reveal that m/z 74 ions came from fragmentation in the EI source, whereas m/z 73 ions came from fragmentation of higher mass ions in the trap.

Overview of Dissertation

This dissertation presents the development and characterization of QITMS instrumentation for ion injection and study of selective ion/molecule reactions. Chapter 2 discusses details of the two instruments used for this work and lists important experimental parameters which were optimized for these instruments. Chapter 3 includes calculations for predicting differences in reaction products and presents results of several types of ion/molecule reactions studied to seek enantioselectivity within the gas phase. Chapter 4 reviews ion/molecule reactions used to study the effects of residual water in the vacuum chamber on ion trap spectral quality and measure the level of water within an

operational QITMS. The final chapter summarizes this work and presents ideas for future applications of this instrumentation.

CHAPTER 2
INSTRUMENTATION FOR ION INJECTION

General Overview

Two QITMS instruments were used for the studies presented in this dissertation. The first instrument described below is a commercial QITMS, the Finnigan GCQ. The second instrument described below was a prototype QITMS instrument (affectionately named SweetP) constructed of parts from a variety of sources. The SweetP instrument was originally characterized with a Finnigan ITS 40 ion trap and Finnigan 4500 EI/CI ion source. Due to difficulties in operation and automation of the instrument with these components, they were replaced by Finnigan GCQ components. Modifications to the GCQ instrument control software were made using both Visual C++ and Visual Basic (Microsoft) programs. Finnigan supplied both the instrument source code and a programmable Visual Basic instrument interface for this task. The new computer control of the instrument saved weeks of effort previously spent tuning optics, as well as writing and optimizing scan functions for the ITS 40 instrument control.

The Finnigan 4500 source was not used to generate any data presented in this dissertation and will not be mentioned in the instrumental sections below. The ITS 40 ion trap and data system were used for a much longer period of time than the TSQ source. Early experiments conducted with the ITS 40 ion trap and data system were easily reproduced once the GCQ ion trap and data system were installed. The ITS 40 ion trap

was used to generate ion/molecule data, presented in Chapter 3, which were not reproduced with the GCQ QITMS in SweetP due to unavailability of acetonide reagents.

Instrument Design

Commercial QITMS: Finnigan GCQ

The GCQ is a QITMS instrument designed for routine GC/MS and GC/MS/MS analysis. The vacuum chamber is pumped by one of two pumps: either a 100 l/s diffusion pump (Edwards SI100) or a 250 l/s turbomolecular drag pump (Edwards EXT 250H). The GCQ is designed to admit the GC effluent into the chamber via a heated transfer line through either the right or left side of the instrument directly into the ion volume of the EI/CI ion source. Three electrostatic lenses are positioned between the source and the quadrupole ion trap to focus and gate ions from the ion volume into the entrance endcap electrode. The controlling electronics surround the vacuum chamber. The RF transformer coil is housed in a cavity integral to the chamber. A personal computer houses interface cards (Acquisition DSP, Control DSP, and Waveform DDS) for communicating with the GCQ electronics.

The GCQ vacuum system is composed of a cast aluminum manifold and machined aluminum top cover plate. The top cover plate is designed to hold the source, lenses, ion trap, and multiplier. This can be removed from the instrument housing for easy maintenance of the working components. The vacuum pump options for the GCQ mentioned above were investigated to obtain pumping speeds for several gases present in the GCQ chamber. Table 2-1 lists the results of these tests. The measured pumping speeds for the EXT turbo pump are about 25% lower than the specifications because the

pump had a splinter shield over the mouth. Although the pump is sold with the splinter shield in place, Edwards does not use the shield when making their pumping measurements.

Table 2-1: Pumping speed measurements and manufacturer's specifications for two Edwards pumps on the GCQ.

	Diffusion Pump (SI 100)		Turbomolecular Pump (250 H)	
Gas	Experimental (L/s)	Specification (L/s)	Experimental (L/s)	Specification (L/s)
Methane	91 ± 2	80	177 ± 4	-
Helium	98 ± 4	100	178 ± 11	230
Nitrogen	74 ± 4	65	163 ± 10	220

Pumping speeds were obtained by multiplying the volumetric flow of the gas into the chamber by the ratio of atmosphere to resultant chamber pressure. Average speeds were calculated for gas flows of 0.3-6.7 atm-ml/min for the diffusion pump and 0.4-9.6 atm-ml/min for the turbo pump. An MKS 390HA capacitance manometer was used to measure the pressure above the pump through the probe lock. The gas flows were measured by difference using two Granville-Phillips series 203 variable leak valves. A J&W ADM1000 flowmeter was plumbed in parallel with the second leak valve supplying the only gas to the instrument. Figure 2-2 shows the experimental setup.

Pumping speed data are useful when considering the gas load that can be placed on the vacuum system before undesirable pressures are reached. The turbo pump's increased pumping speed offers some advantage for chemical ionization by allowing

more gas to be flowed into the source with the same resultant chamber pressure as with lower reagent gas flow into the diffusion pumped instrument. A higher ion source pressure can therefore be maintained for the same chamber pressure.

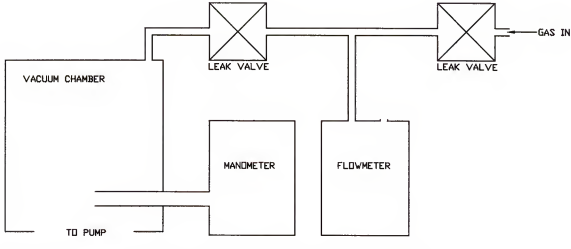

Figure 2-2: Experimental setup for pumping speed measurements.

The following example demonstrates how pumping speed can be used to estimate the chamber pressure for a given gas load. The normal GCQ helium gas load is about 1.6 atm-mL/min or 0.02 Torr-L/s. The GC contributes approximately 1.2 atm-mL/min helium under typical conditions (DB-5, 30m column operated at constant linear velocity of 40 cm/s); the helium buffer gas introduced into the trap contributes approximately 0.4 atm-mL/min (5 psi head pressure on the restrictor discussed below). If the diffusion pump is used, the pressure in the chamber is (0.02 Torr-L/s / 100 L/s) = 2×10^{-4} Torr. An ion gauge calibrated for nitrogen reads 2.9×10^{-5} Torr (using a sensitivity correction factor for helium of 7) for this gas pressure. Likewise, the ion gauge should read about 1.6×10^{-5} Torr in the turbo-pumped instrument.

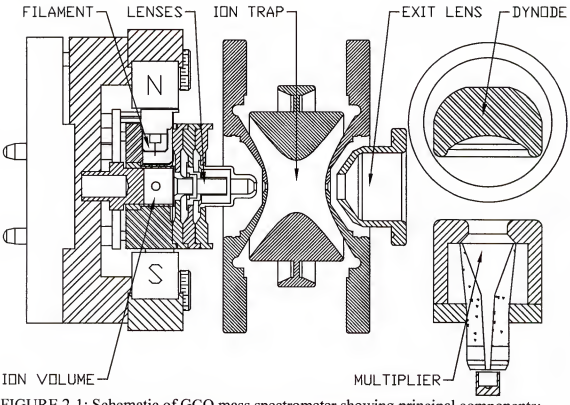

FIGURE 2-1: Schematic of GCQ mass spectrometer showing principal components: EI/CI source, ion optics, analyzer, and detector.

Figure 2-1 shows the principal components of the GCQ QITMS. The EI/CI ion source contains a heated source block (0-225°C) which holds two types of interchangeable ion volumes. One is an enclosed design with a 0.6mm^2 ion exit aperture for CI and the other has a fully open exit designed for EI. Each ion volume has three holes in addition to the ion exit hole. The two 0.090" diameter holes on the sides of the ion volume are plugged with the GC transfer line on one side and a fitting for CI gas and calibration gas on the other. The fourth hole is a 0.015" diameter hole for the electron beam from the filament. The standard filament is a 0.004" diameter rhenium wire rated for 3 watts heat dissipation. A low wattage filament (0.003" diameter, 2 watts) is also available for analyzing samples with less thermal degradation by allowing the source to

operate at a lower temperature. The filament design is different from typical straight or coil designs. It is a hairpin design, with a sharp bend in the filament directly above the electron hole in the source block to emit electrons from a focussed point. The filament assembly also has an electron lens between the filament and the source block. The electron lens serves both to extract the electrons from the filament to keep it from overheating and to focus the electrons into the ion volume. This enables the filament to be operated at electron energies as low as 0 eV with respect to the source and still be able to maintain high emission currents.

The three tube lenses located between the source and the trap extract ions from the source and focus them into a beam to be transmitted into the trap. Lens 2 is also used as a gate to keep ions from being injected into the trap when the instrument is not in the ionization mode. Typical voltages on the lenses for positive EI ions are –22V, -80 V (gate on) / + 100 V (gate off), and -22 V for lenses 1, 2, and 3, respectively, all versus the grounded ion source.

The GCQ ion trap is composed of a ring electrode sandwiched between two endcap electrodes, separated by two silicon nitride insulating spacers. The main RF is applied to the ring electrode at a frequency of 1030 kHz and amplitude of 0-8500$V_{0\text{-}p}$. A resonant ejection voltage is applied to the endcap electrodes at a frequency of 476.375 kHz and amplitude of 0-30 $V_{p\text{-}p}$. The upper m/z limit of the GCQ mass analyzer is 1000 m/z with these voltage settings. A direct current (DC) offset of 0-±10 V is applied to the ion trap electrodes with respect to the source to attract ions. This is typically -10 V for positive EI and CI, and +3-+7 V for negative CI. Helium buffer gas is added to the trap

at a pressure of 1 mTorr to collisionally dampen (cool) the oscillations of the injected ions to the center of the trap and improve detection.

The exit lens located between the exit endcap and the dynode helps isolate the ion trap from the strong potential field of the dynode and focus the ions exiting the ion trap. Varying the potential on this lens has little effect on the sensitivity of detection. The potential is therefore set to ground.

The GCQ detector assembly consists of a conversion dynode and continuous-dynode electron multiplier. The dynode is biased at ±15 kV, with the polarity opposite that of the ions being analyzed. Ions strike the dynode and emit secondary ions and electrons, which are accelerated to the multiplier. Particles from the dynode strike the surface of the electron multiplier with enough energy to cause secondary emission of electrons from the multiplier surface. The secondary electrons in turn cause emission of more electrons as they are drawn down into the more positive funnel of the multiplier towards the grounded anode. This cascading of electrons causes a gain in current for detection. The multiplier is optimized for a gain of 3×10^5 by varying its potential between -900 and -3000 V at the cathode. The multiplier anode, the cup located at the base of the multiplier, collects the electrons emitted by the cathode, passing the current to the electrometer.

Differentially Pumped QITMS: SweetP

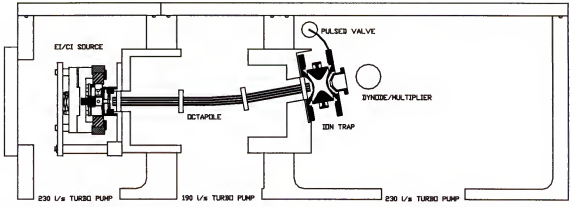

FIGURE 2-3: Side view of SweetP instrument showing location of EI/CI ion source, ion optics, ion trap, pulsed valve, and detector within the differentially pumped manifold.

The vacuum manifold for the differentially pumped SweetP instrument, shown in Figure 2-3, is sand-cast aluminum with a glass top cover. It contains three distinct chambers separated by adjustable baffle walls. The first chamber houses the EI/CI ion source and is pumped by a Pfeiffer Balzers TPH 240H turbomolecular pump. The ion gauge in this chamber reads in the low 10^{-5} Torr range with GC helium being introduced. The Varian 3400 GC on the source is not capable of constant flow or velocity modes. The flow is set by manually adjusting the head pressure, so the chamber pressure varies considerably depending upon the column temperature. The second chamber houses the transmission RF octapole and is pumped by a Pfeiffer Balzers TPH 190 turbomolecular pump. There is not typically an ion gauge on this chamber; however, in one test, the chamber pressure was raised to 1×10^{-3} Torr with helium before significant loss in sensitivity was detected. The third chamber is pumped by a Pfeiffer Balzers TPH 240 turbomolecular pump and holds the analyzer and detector. Under normal operation with

1 mTorr helium buffer gas, this chamber maintains an uncorrected pressure of 3.3×10^{-6} Torr. Base pressure for the first and third chambers without helium is 9×10^{-8} Torr.

A GCQ EI/CI source is mounted in the SweetP instrument. Only a few modifications were needed for the source to fit in the instrument. New mounting brackets were made, and the lens stack was modified. Several modifications were made to ion volumes for ionization methods other than normal GC/EI/CI. For some solid samples, the backs of ion volumes were drilled out for placement of the solids or direct exposure probes. For some samples, MALDI and LDCI techniques were used. For the laser techniques, the ion volumes were modified by mounting a sample plate perpendicular to the transfer line hole on the base of the ion volume. A 1" diameter flange mounted in the Cajon coupling replaced the GC transfer line. The flange contained an o-ring groove cut to hold a laser window in place over the o-ring while under vacuum. To control the laser pulse from the GCQ electronics, TTL signals from U68 on the GCQ main board were used. Pin 3 of U68 triggers the laser during the first half of ion injection in full scan (full scan has two consecutive injection events), and during the entire ionization time in SIM and MS/MS mode.

The SweetP instrument has three electrostatic lenses between the ion source and the octapole. Lens 1 is a standard GCQ lens 1. This is kept unchanged to keep the extraction potentials similar between instruments for comparative purposes. Lens 2 is a thick flat lens with a slightly larger inner diameter than the outer diameter of lens 1. A spacer is placed between lens 1 and 2 to make the entire lens assembly thicker than the heater cartridges upon which the lenses are mounted. This keeps the heaters from being

pressed against the baffle wall. Lens 3 is the gate lens and octapole entrance lens. Lens 3 is a thin flat lens. Typical voltages on the lenses for positive EI ions are –20V, -130 V, and -130 V (gate on) / + 100 V (gate off) for lenses 1, 2, and 3, respectively.

The octapole has a 10° bend to keep high-energy neutrals, photons, and electrons produced in the ion source from accidental transmission into the trap while still transmitting ions into the trap. The octapole is approximately 9 inches in length with an r_0 of 0.11". A Finnigan TSQ 45 lens voltage power supply is used to set the amplitude of the octapole RF on a separate prototype RF amplifier made by Finnigan. A –8.0V setting represents an amplitude of 800 $V_{0\text{-}p}$ at the octapole, which is the recommended upper limit for the amplifier. The octapole does exhibit some mass discrimination based upon RF amplitude, but at an amplitude of 200-500$V_{0\text{-}p}$ and frequency of 2.475MHz, it transmits the entire mass range of ions able to be analyzed by the GCQ QITMS. Low amplitudes favor transmission of low m/z ions, whereas high amplitudes favor transmission of high m/z ions. The octapole potential is offset from the source by a DC potential of 0-±30 V (TSQ 45 lens supply, 3L1). It is most efficient at the full ±30 V offset.

A GCQ ion trap is currently mounted in the SweetP instrument. The prototype instrument used for tests at Finnigan had an ITS 40 ion trap mounted to the second baffle wall. The ITS 40 ion trap was used along with ITS 40 electronics for some time on the SweetP instrument before switching to the GCQ ion trap and electronics. A modified gate circuit, resonant excitation waveform amplifier, and balun were made to allow the ITS 40 electronics to analyze both positive and negative ions with ion injection, as well

as to perform CID and single ion isolation using forward and reverse scans. The waveform amplifier and balun were adapted from GCQ electronics. The gate circuit was modified to allow the gate lens potential to be controlled by Finnigan 4500 power supplies (quadrupole electronics module and ion control module). The 4500 power supplies also controlled source voltages, heaters, and filament current. The scan functions for control of the ion trap were written using Gatorware software (Griffin, 1995). The DC offset applied to the SweetP ion trap is typically −13 V for positive EI. The range for trap offset is ±10 V when using the GCQ software and electronics, but this can be extended beyond ±30 V using the custom GCQ software.

The detector for SweetP is a dynode and De Tech continuous-dynode electron multiplier assembly similar to the GCQ. The dimensions of the conversion dynode and electron multiplier are only slightly different from the GCQ, but they function the same and operate with the same voltages as the GCQ dynode/multiplier assembly.

The SweetP instrument is fitted with a pulsed valve plumbed directly into the gas feed of the exit endcap with 1/16" stainless tubing. This pulsed valve is controlled by a custom built controller triggered by TTL signals from the GCQ main board U68 pin #7 (it was also triggered by programmable TTL signals on the ITS 40). The pulsed valve controller contains a monostable circuit that will not allow the valve to remain on for more than 15 ms unless the monostable time constant is changed. This protects the valve from burning out in case the TTL accidentally becomes stuck in the active position. The TTL signal is controllable within the custom software used to operate SweetP in MS/MS mode. The source code was modified to provide a complete time event dedicated to the pulsed valve after the first isolation event in MS/MS and before the CID activation event.

Ions can be isolated then neutrals can be pulsed in for a determined pulse time, and the reaction time with the neutrals can be set by the resonant excitation time. By adjusting the excitation amplitude to 0 V, the resonant excitation event becomes just a time delay event. The reaction products can be studied either by full scan, looking at a wide mass range for product ions in MS/MS mode, or by MS/MS in mode MS^3, by selecting products and resonantly exciting them in another stage of MS/MS directly after the reaction event.

Characterization of GCQ and SweetP Instrument Parameters

Injection RF Level

The injection IonRf must be optimized for efficient trapping of all ions within the QITMS. The injection IonRf compensates for differences in ion momenta entering the ion trap (March and Hughes, 1989). Higher injection IonRf levels increase the potential for oscillatory motion in the trap. Ions of different m/z accelerated over the same potential gradient from the source will have the same kinetic energy; however, their momenta will change with the square root of their m/z, as shown below (2-5). Therefore ions of greater m/z will require higher injection IonRf to convert forward momentum into oscillatory motion within the ion trap. If the injection IonRf is raised too high, however, ions will be excited too much and not be trapped. As mentioned in Chapter 1, ions of m/z below the injection IonRf level will definitely be ejected from the trap during injection, limiting the m/z range of ion stored. Consider a single ion of m/z m_1 and a second ion of m/z m_2, each accelerated into the ion trap with the same kinetic energy (2-1). The following equations derive the relationship between the momenta (mv) of these ions:

$$\tfrac{1}{2} m_1 v_1^2 = \tfrac{1}{2} m_2 v_2^2 \quad (2\text{-}1)$$

Solving for the ratio of momenta,

$$(m_1 v_1)/(m_2 v_2) = v_2/v_1 \quad (2\text{-}2)$$

taking the square root of both sides of 2-2,

$$\sqrt{m_1 v_1 / m_2 v_2} = \sqrt{v_2 / v_1} \quad (2\text{-}3)$$

solving for v_2/v_1,

$$\sqrt{m_1 / m_2} = v_2 / v_1 \quad (2\text{-}4)$$

and substituting into 2-2,

$$\sqrt{m_1 / m_2} = (m_1 v_1)/(m_2 v_2) \quad (2\text{-}5)$$

This becomes useful when determining the optimal IonRf level for injection of ions. To tune the QITMS injection IonRf for a given set of conditions such as trap offset and trap pressure, tune curves of intensity versus injection IonRf such as in Figures 2-4 and 2-5, are made for a series of ions over the m/z range of the QITMS. The optimal IonRf for each ion is recorded as the IonRf that gives the maximum signal intensity for that ion. By plotting the optimal injection IonRf versus the square root of m/z, a linear equation of the form $y = mx + b$ is generated where x is the square root of m/z and y is the optimal IonRf for injection. For the GCQ this equation is given in the instrument initialization file, by default, as $y = 1.65x + 3$. For SweetP at –13 V trap offset and 1 mTorr trap pressure, this equation is $y = 2.8x + 5$. The optimal injection IonRf increases with increasing trap offset. Figure 2-4 shows that the leading edge of ions detected increases in IonRf with increasing DC trap offset voltage. This can account for the higher values for the SweetP instrument, since the trap offset optimizes at 13 V on the SweetP

instrument, whereas the GCQ trap offset is set to 10 V by default and is limited to 10 V in the commercial software.

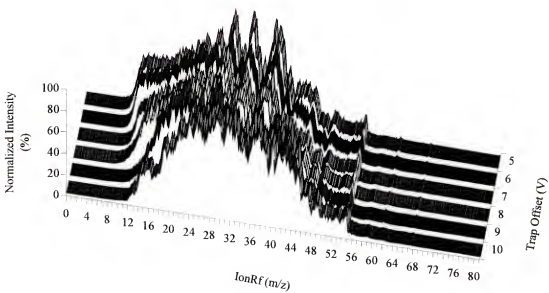

FIGURE 2-4: Chart showing effects of DC trap offset voltage and IonRf on the injection of benzene ions (m/z 78).

The fine structure in these IonRf tune curves is similar to that reported by others (Yost and Pedder, 1989). They may be due to non-linear resonances from distortions of the hyperbolic trapping field which decrease trapping efficiency (Dawson and Whetten, 1969).

Some ions do not follow the trend of increasing injection IonRf with increasing m/z; rather, they optimize at a higher injection IonRf than expected. These ions are either fragment ions or products of ion molecule reactions in the ion trap. For example, the CF_3^+ (m/z 69) and $C_3F_5^+$ (m/z 131) fragment ions of FC43 are common fragments of most

higher m/z FC43 ions and thus have broad injection IonRf profiles. Methyl stearate shows injection IonRf profiles for two ions similar in m/z that optimize in different IonRf ranges (Figure 2-5).

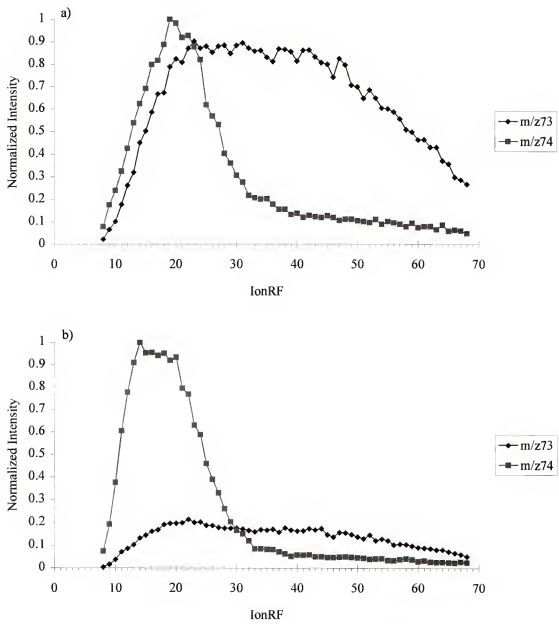

Figure 2-5: Normalized Intensity versus IonRf for methyl stearate fragment ions in the GCQ with different neutral methyl stearate pressures in the GCQ chamber. a) Methyl stearate at a background-subtracted (uncorrected) ion gauge pressure of 5.3×10^{-5} Torr; b) Methyl stearate at a background-subtracted (uncorrected) ion gauge pressure of 3×10^{-6} Torr.

In Figure 2-5, the fragment ion at m/z 73 ion ($CH_2COOCH_3^+$) begins to be trapped at a higher IonRf than the higher m/z 74 ion ($[CH_2COOCH_3 + H]^+$), and continues to be detected at IonRf values over 60. This is above the optimal injection IonRf of the molecular ions (IonRf ~ 35-40). The m/z 73 ion is most likely a fragment ion of the product of a condensation ion/molecule reaction involving higher m/z ions and neutrals. The intensity of m/z 73 increases relative to m/z 74 with increasing concentration of neutral methyl stearate in the ion trap, as shown in Figure 2-5, where neat methyl stearate was placed in the chamber and the IonRf tune curves were acquired as the methyl stearate pumped away. In this example, the IonRf tune curve is flat at high IonRf because of neutrals making their way into the ion trap to cause ion/molecule reactions. When optimizing the IonRF it is best to use ions that exhibit sharp IonRf profiles such as m/z 74 and not m/z 73.

Ion Optics

The ion optics for both instruments are described above. Tuning of the GCQ electrostatic lenses and trap offset is explained within the software manuals. The SweetP instrument requires manual tuning not possible within the standard GCQ software. A typical lens tune on the SweetP instrument involves first tuning the octapole, then trap offset and lens stack, and then repeating the process until a desirable tune is obtained. Because all ion optics are integral in the tune, good default values must be used to start. When low m/z ions will be investigated, the octapole RF amplitude is set to 200 $V_{0\text{-}p}$ (-2 V on the TSQ 45 lens supply, 2L3) or less. For high m/z ions, the octapole amplitude is set to 500 $V_{0\text{-}p}$ (-5 V, 2L3). A good starting point for all m/z ions is 300 $V_{0\text{-}p}$. A series of

stopping potential experiments were done varying the DC offset of the octapole with respect to the source. It was discovered that most ions were not transmitted below a -10 V offset for positive ions and a +10 V offset for negative ions. Optimal transmission occurs from ±14-±30 V offset. The SweetP lenses require tuning outside the limits set by the standard GCQ software, so they must be tuned using the custom software. A tune file can be saved from the custom software that can then be used to set the lens voltages within the GCQ software. When tuning the lenses, it is a good idea to choose both stable ions and fragment ions and tune for gentle ion injection. The fragment ions will give an idea of where the injection energies become too high. Figure 2-6 shows the results of a trap-offset tune on the SweetP instrument in positive CI mode using FC43. The m/z 414

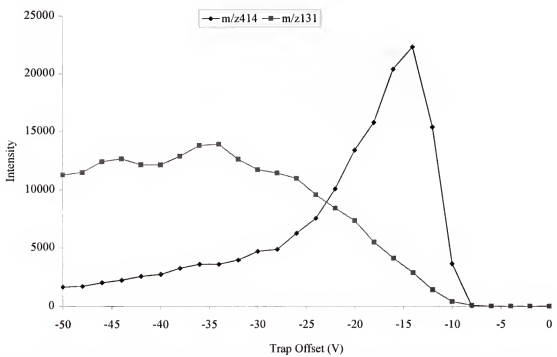

Figure 2-6: PCI tune of trap offset voltage on SweetP showing stable and fragment ions.

ion is a relatively stable ion. The m/z 131 ion results from fragmentation of other ions in the trap, primarily m/z 219, m/z 434 and m/z 614. It is not produced by CI.

Helium Buffer Gas

The pressure within the GCQ trap is set by adjusting the inlet helium pressure on a 6" long fused silica capillary restrictor. The flow of helium through the capillary can be obtained by equations 2-6 through 2-7 (Thompson, 1994). The helium viscosity is

$$\eta = 4.05\times10^{-7}\,T + 7.58\times10^{-5} \qquad (2\text{-}6)$$

where

η = helium viscosity, dyn×s/cm^2

T = temperature, K

Average linear velocity through the capillary into vacuum is

$$V_{avg} = \frac{3(r/2)^2(P+14.7)\times 68947}{32\eta\times L} \qquad (2\text{-}7)$$

where

V_{avg} = average linear velocity, cm/s

r = capillary inner radius, cm

P = capillary inlet pressure, psi (atmospheric)

L = capillary length, cm

The flow (ml/min) is then

$$F = 60\pi(r^2)V_{avg}\times\left[\frac{298}{T}\right]\times\left[\frac{2(P+14.7)}{3\times14.7}\right] \qquad (2\text{-}8)$$

Table 2-2 shows the results of theoretical calculations for the flow through this capillary at several different head pressures and two different capillary diameters. A

capillary restrictor was calibrated by applying a high pressure to the capillary to obtain a measurable flow and measuring the flow with a flowmeter. Then the actual diameter was calculated knowing the temperature, length, and head pressure on the restrictor. The first diameter in Table 2-2 is the actual calibrated diameter (0.00553 cm) for this restrictor, while the second diameter is the manufacturer's reported diameter (0.0050 cm, uncalibrated). The restrictor inner diameter differs from the manufacturer's quoted diameter by about 10 % as the calibration revealed. The results of the helium flow calculations indicate that the flow varies considerably based upon the actual diameter of the restrictor.

Table 2-2: Calculated helium flow through a 6" capillary restrictor at 25°C.

Capillary Inner Diameter (cm)	0.00553	0.0050
Pressure (psi)	Flow (ml/min)	
-1	0.201	0.134
0	0.231	0.154
1	0.264	0.176
2	0.298	0.199
3	0.335	0.224
3.5	0.354	0.237
4	0.374	0.250
4.5	0.394	0.263
5	0.415	0.277
5.5	0.436	0.292
6	0.458	0.306
6.5	0.481	0.321
7	0.503	0.336
7.5	0.527	0.352
8	0.551	0.368
8.5	0.575	0.385
9	0.601	0.401
9.5	0.626	0.418
10	0.652	0.436

The conductance out of the GCQ ion trap for helium was calculated to be 3.736 L/s by Jae Schwartz at Finnigan. Therefore, at a head pressure of 5 psi the flow is approximately 0.3 ml/min in Table 2-2, and the trap pressure at room temperature should be approximately:

$$(.3/60000)\ \text{L/s} \times 760\ \text{Torr}/ (3.7\ \text{L/s}) = 1\ \text{mTorr} \qquad (2\text{-}6)$$

A capacitance manometer was used to make trap pressure measurements without the GC attached to the GCQ. Initial measurements suggested the trap pressure was somewhat lower than calculated; however, loose Teflon tubing was to blame. The Teflon tubing between the helium restrictor and trap, and between the capacitance manometer and trap was replaced with stainless steel tubing and the measurements confirmed that the trap pressure was indeed .98-1.01 mTorr at 5 psi head pressure on the capillary restrictor.

Figure 2-7 shows the effects on the trap offset tune curve shown in Figure 2-6 at three different trap pressures. Although the signal intensity increases with increasing trap pressure, there are several disadvantages to raising the trap pressure much above 2mTorr. One disadvantage is that the time between analyte and helium collisions decreases so that the resonant excitation cannot accelerate the ions sufficiently before a collision to give them enough kinetic energy to fragment from the collision (Brodbelt, 1995). Excess collisions with the buffer gas may actually help to remove energy from the ions, decreasing their ability to fragment. Another drawback is the increased amount of water admitted into the trap with higher buffer helium flow rate, which can lead to an increase in ion/molecule reactions with water. Finally, chamber pressure increases making the evacuation of the source less effective.

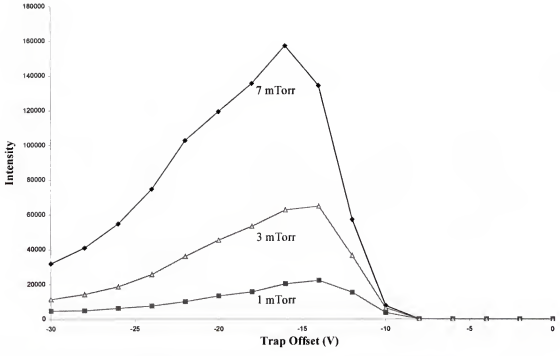

Figure 2-7: Graph showing the effects of trap helium pressure on intensity of m/z 414 ions produced by positive CI during a trap offset tune on the SweetP instrument.

Resonant Excitation Voltage

The GCQ is calibrated to perform resonant excitation over a small frequency range. In order to expand the capabilities of the SweetP instrument for resonant excitation at all possible frequencies, the balun and waveform amplifier were calibrated to output known amplitudes at frequencies from 83-1331 kHz. A function was programmed into the custom software to compensate for the gain of the waveform circuitry at any given resonant excitation frequency during MS^n. The gains of balun and waveform amplifier were tested to produce the calibration function by applying waveforms from a Stanford Research Systems DS 345 (Sunnyvale, CA) arbitrary waveform generator at

various frequencies and amplitudes. The gain (V_{out}/V_{in}) was found to be a function of the frequency, but independent the amplitude of the input voltage, V_{in} (Figure 2-8).

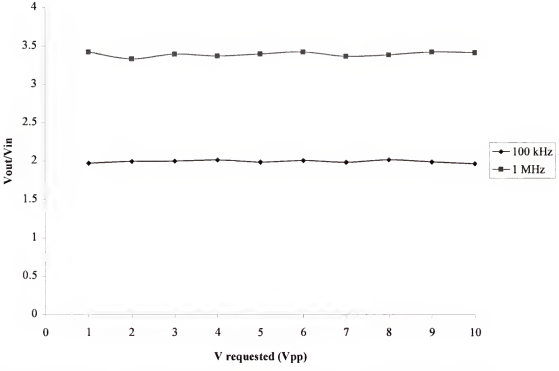

Figure2-8: Vin/Vout values versus requested SRS Vpp at 100 kHz and 1 MHz.

The gain of the entire frequency circuit from the waveform DDS card in the computer to the endcap electrodes was measured for a number of excitation frequencies. The gain is represented by the slope of each series in Figure 2-9. The gain values were then plotted versus frequency and fit to a sixth-order polynomial (Figure 2-10). This polynomial equation is used to determine the gain for each frequency selected in MS/MS. When an excitation amplitude is selected, the software adjusts the requested amplitude sent to the waveform DDS so that the endcap voltage matches the user requested amplitude.

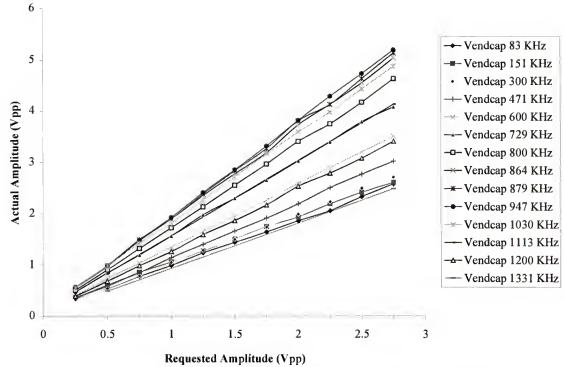

Figure 2-9: Resonant excitation amplitude versus requested amplitude at several frequencies.

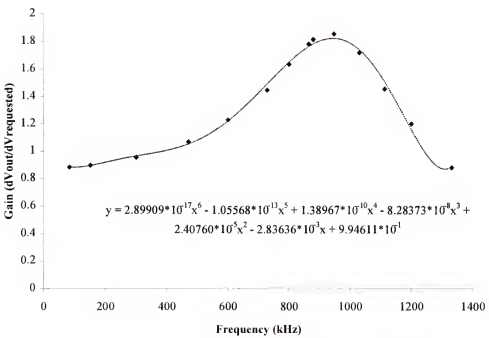

Figure 2-10: Gain versus frequency for resonant excitation amplitude.

Tuning the GCQ Electronics for CI

Because the masses of the ions produced from FC43 are different in EI and CI, it is necessary to choose new masses to tune for CI in the automatic tune software. In negative methane CI of FC43, there are numerous ions at many masses available for

Table 2-3: Mass list of ions commonly seen in negative methane CI of FC43.

Exact m/z	Nominal m/z	Formula	Exact m/z	Nominal m/z	Formula
34.9689	35	Cl^-	368.9823	369	$C_9F_{13}N^-$
36.9659	37	Cl^-	375.9807	376	$C_8F_{14}N^-$
69.9378	70	Cl_2^-	382.9791	383	$C_7F_{15}N^-$
71.9348	72	Cl_2^-	387.9807	388	$C_9F_{14}N^-$
73.9318	74	Cl_2^-	394.9791	395	$C_8F_{15}N^-$
78.9183	79	Br^-	395.98693	396	$C_8F_{15}NH^-$
80.9163	81	Br^-	401.9775	402	$C_7F_{16}N^-$
126.9045	127	I^-	406.9791	407	$C_9F_{15}N^-$
151.9935	152	$C_2F_6N^-$	413.9775	414	$C_8F_{16}N^-$
168.9888	169	$C_3F_7^-$	425.9775	426	$C_9F_{16}N^-$
206.9919	207	$C_2F_7N^-$	432.9759	433	$C_8F_{17}N^-$
213.9903	214	$C_4F_6N^-$	433.98373	434	$C_8F_{17}NH^-$
218.9856	219	$C_4F_7^-$	444.9759	445	$C_9F_{17}N^-$
225.9903	226	$C_3F_8N^-$	451.9743	452	$C_8F_{18}N^-$
230.9856	231	$C_3F_9^-$	463.9743	464	$C_9F_{18}N^-$
232.9887	233	$C_4F_9N^-$	475.9743	476	$C_{10}F_{18}N^-$
244.9887	245	$C_5F_9N^-$	482.9727	483	$C_9F_{19}N^-$
256.9887	257	$C_6F_9N^-$	494.9727	495	$C_{10}F_{19}N^-$
263.9871	264	$C_5F_{10}N^-$	501.9711	502	$C_9F_{20}N^-$
275.9871	276	$C_6F_{10}N^-$	506.9727	507	$C_{11}F_{19}N^-$
282.9855	283	$C_5F_{11}N^-$	513.9711	514	$C_{10}F_{20}N^-$
283.99333	284	$C_5F_{11}NH^-$	518.9727	519	$C_{12}F_{19}N^-$
294.9855	295	$C_6F_{11}N^-$	525.9711	526	$C_{11}F_{20}N^-$
301.9839	302	$C_5F_{12}N^-$	532.9695	533	$C_{10}F_{21}N^-$
311.9871	312	$C_9F_{10}N^-$	544.9695	545	$C_{11}F_{21}N^-$
313.9839	314	$C_6F_{12}N^-$	556.9695	557	$C_{12}F_{21}N^-$
325.9839	326	$C_7F_{12}N^-$	575.9679	576	$C_{12}F_{22}N^-$
330.9855	331	$C_9F_{11}N^-$	582.9663	583	$C_{11}F_{23}N^-$
332.9823	333	$C_6F_{13}N^-$	587.9616	588	$C_{11}F_{24}^-$
337.9839	338	$C_8F_{12}N^-$	594.9663	595	$C_{12}F_{23}N^-$
344.9823	345	$C_7F_{13}N^-$	613.9647	614	$C_{12}F_{24}N^-$
349.9839	350	$C_9F_{12}N^-$	632.9631	633	$C_{12}F_{25}N^-$
351.9807	352	$C_6F_{14}N^-$	633.97093	634	$C_{12}F_{25}NH^-$
356.9823	357	$C_8F_{13}N^-$	670.9599	671	$C_{12}F_{27}N^-$
363.9807	364	$C_7F_{14}N^-$	682.9599	683	$C_{13}F_{27}N^-$

tuning lenses. Table 2-3 lists these masses as well as chloride, bromide, and iodide ions, which are usually present and help in tuning the low m/z range.

At low CI reagent pressures it is common to see ions produced by both EI and CI. Ions produced by CI and not by EI should be chosen to optimize the tune for CI ions. The ion at m/z 452 is also an abundant ion in negative EI and should not be used for lens and reagent pressure tuning. Ions near m/z 70 should not be used for mass calibration, because it is often difficult to discern between isotopes of CF_3, Cl_2, and HCl_2 when the mass calibration is off. The CF_3 and HCl_2 ions are not common; however, HCl_2 ions can be observed after some chlorinated pesticides have contaminated the ion source.

In positive methane CI, the following FC43 ions are produced primarily by CI: m/z 434, 564, 576, 602, 614, and 652. A prominent ion at m/z 414 was not included in this list because it is also an abundant ion in EI. These ions may be used for lens tuning. Unfortunately, they do not offer sufficient low m/z ions for mass calibration.

Due to the higher chamber pressure in CI, the ion trap needs minor changes in mass calibration when switching from EI to CI. The best way to assure an accurate mass calibration in CI is to manually tune the instrument on ions present in CI. The following procedure is simple to perform. Open the Inst.ini file in the C:\GCQ\bin directory and obtain the mass calibration parameters under the CI Calibration heading called mslope and mintercept. These parameters are used to assign a mass to each DAC of acquired data (equation 2-7).

$$DAC = m/z \times mslope + mintercept \qquad (2\text{-}7)$$

Use equation 2-7 to calculate the DAC values for a series of ions visible in the tune window whose exact masses are known. Plot the DAC values versus the exact masses to obtain a new mslope and mintercept. Enter the new mslope and mintercept into the inst.ini file, save it, and reload the instrument software. For example, assume an ion is visible at m/z 100.0 in the tune window and the current calibration lists mslope = 63.5 and mintercept = 150. The DAC value is 6500 for the m/z ion whose exact mass is actually 99.9936. Thus the (x,y) data to be plotted for the new calibration will include the point (99.9936, 6500).

Optimization of CI Parameters

The optimization of source pressure, electron energy, and emission current is necessary to do good CI within the GCQ ion trap instruments with ion injection. Every type of ion source has different characteristics when it comes to CI, so the GCQ source conditions discussed below do not apply to other types of mass spectrometers. These parameters must be adjusted properly to obtain good sensitivity in these instruments.

There is no easy way to use the ion gauge reading on the chamber to set the source pressure in CI unless the GC chromatographic conditions and the source temperature remain constant. Also, ion gauge readings vary from instrument to instrument. The best way to assure known pressure is to measure the source pressure with the capacitance manometer probe before each new experiment. Figure 2-11 shows source pressure and methane flow in a GCQ instrument at Finnigan (Austin,TX) for both vacuum pump options. The flows were measured using two Granville-Phillips variable leak valves in series for differential measurements as mentioned above for the pumping

speed calculations. The ion gauge used for this plot was calibrated to read helium pressure. To convert the ion gauge readings in Figure 2-11 for air calibration, the reported pressures must be divided by 5.5. This is the manufacturer's sensitivity correction for the Granville-Phillips mini ion gauge used in this study. This figure may not accurately reflect ion gauge readings on both Florida instruments, but it is useful for seeing the relationship between flow and source pressure.

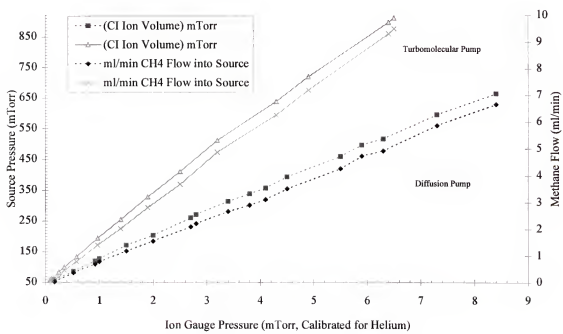

Figure 2-11: GCQ total ion source pressure and methane flow versus ion gauge pressure (with approximately 1.3 ml/min helium flow into the source and 5 psi helium on the capillary restrictor into the trap).

Most reports on CI for other types of instruments suggest that the source pressure and electron energy must be high (typically 0.3-1 Torr and 70-400 eV) to perform good CI (Harrison, 1992; Stemmler and Hites, 1988). The following figures show that the

GCQ source and ion trap are most sensitive at moderate source pressures and 70 eV electron energy. While the signal intensity increases with increases in electron energy (Figures 2-12 and 2-13), source pressure (Figures 2-14 and 2-16), and emission current (Figures 2-17 and 2-18), the signal-to-noise tends to decrease as these parameters are increased. Sensitivity may be measured as signal-to-noise (Chapman, 1994). The signal-to-noise values that follow were calculated automatically for mass chromatographic peaks in the GCQ data system.

There is a tendency to want to tune the instruments for greater signal intensity, but this can reduce the dynamic range and signal-to-noise. The ion trap is limited by the number of ions that can be trapped. The number of ions to be injected into the ion trap is controlled by the software, as mentioned below. If the ion trap is able to fill with analyte ions, any increase in ionization efficiency of background will only reduce the number of analyte ions that can be held in the trap. The signal-to-noise ratio is a good measure of the sensitivity of the instrument. If the intensity of an ion increases, but the noise increases even more, the sensitivity is decreased. This is an important aspect of trace analysis that must be grasped: when limits of detection are important, the signal-to-noise should be optimized, not total signal intensity. Figure 2-12 shows that the intensity of FC43 ions in CI is greatest near 200 eV, but by looking at fixed concentrations (GC injections) of ions such as the $[M+H]^+$ ion of decafluorobenzophenone in Figure 2-13, the signal-to-noise actually decreases as the peak intensity increases. A sharp decrease in sensitivity was noticed for both positive and negative ions regardless of concentration on both the GCQ and the SweetP instrument as electron energy was raised. At higher electron energies, not only are more analyte ions being made, but more background ions

are being made as well. Furthermore, electrons have more energy to penetrate through the high pressure source and more EI can take place in addition to CI. The ion trap is limited by the total number of ions it may hold, so that the range of analyte ions able to be stored is decreased as other ions fill the trap.

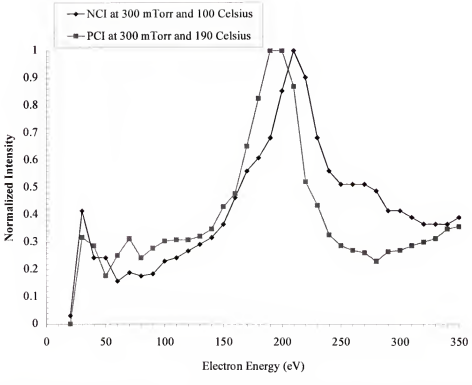

Figure 2-12: Normalized Intensity versus electron energy for the sums of positive (m/z 434, 564, 576, 602, 614, and 652) ions and negative (m/z 557, 595, 633, and 683) ions of FC43 produced by methane CI and analyzed in SIM mode.

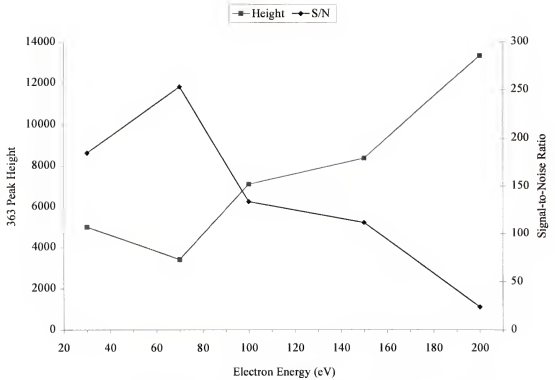

Figure 2-13: Mass peak height and signal-to-noise ratio versus electron energy for decafluorobenzophenone $[M=H]^+$ ions produced by methane PCI (400 mTorr, single injections of 100 pg).

Increasing the source pressure above 300 mTorr does not offer any improvement in sensitivity for the GCQ and SweetP instruments for the compounds studied. Figure 2-14 demonstrates that the signal intensity in methane CI is greatest between 300 and 400 mTorr total source pressure. As the pressure is raised, the mass resolution can be affected, as shown in Figure 2-15 by the increased peak width as the pressure is increased. Figure 2-16 shows that the signal-to-noise is not improved when the source pressure is increased above 150 mTorr for decafluorobenzophenone $[M+H]^+$ ions, even though the signal intensity is increased five-fold when the pressure is increased from 150 mTorr to 450 mTorr.

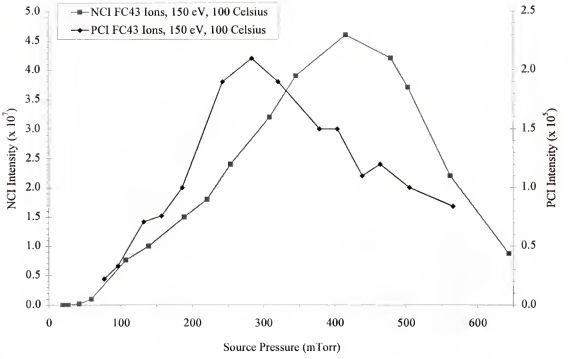

Figure 2-14: Intensity versus source pressure for FC43 negative (m/z 557, 595, 633, and 683) and positive ions (m/z 434, 564, 576, 602, 614, and 652) produced in methane CI.

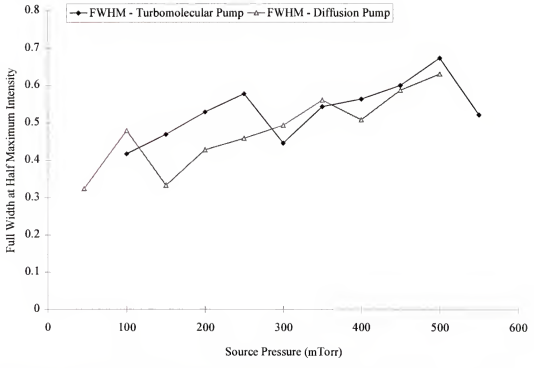

Figure 2-15: Hexachlorobenzene $[M+H]^+$ ion (m/z 285) peak width versus source pressure in methane positive CI (single injections of 200ng).

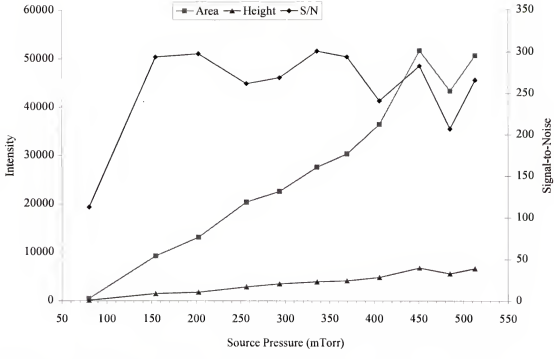

Figure 2-16: Peak intensity, area, and signal-to-noise versus source pressure for decafluorobenzophenone $[M+H]^+$ ions in positive methane CI.

The source pressure should be chosen to efficiently produce the ions under study, with the lowest loss in resolution for the best signal-to-noise. If the signal-to-noise is good, the intensity of ions in the trap can be adjusted by changing the ion injection time, having a similar effect as increasing the source pressure, but without the added gas load. The final test for good source pressure is then to produce a calibration curve and determine whether the signal-to-noise, sensitivity, linear dynamic range and limit of detection are acceptable. For some compounds, the source pressure may need to be higher than for other compounds to maintain an appropriate ratio of reagent ions to analyte. This is a parameter that requires particular optimization for each compound.

In trace analysis employing negative CI, the best limits of detection and signal-to-noise were found by setting the reagent gas pressure to minimize the number of background ions filling the trap. To properly set the pressure for maximum sensitivity in negative methane CI, the calibration gas must first be turned off and allowed sufficient time to be removed from the chamber, so that it does not make up the majority of the background. The source temperature should be at a minimum stable temperature. (Source temperature is usually set to minimize the thermal degradation of the analyte and yet keep the source hot enough to remain clean. In negative CI the best sensitivity for molecular anions is usually obtained with a low source temperature, such as 100°C. Due to the higher concentrations that are typically injected in positive CI and EI, the source temperature is usually set as high as possible to keep the source clean and the signal reproducible.) Lens voltages, trap offset, IonRf, and mass range are set to the values that will be used for the analysis. These values may be readjusted once the reagent pressure has been set, and the process repeated. Next, the methane valve is slowly opened until background ions are observed. (There should be no signal until the methane is introduced, because negative EI is not efficient enough to detect normal background.) The methane pressure is raised until the trap becomes filled close to the target level set within the tune software (AGC target = 5-1). This point is marked by a sudden decrease in ionization time from the maximum iontime (25 ms in normal software). Finally, the methane pressure is lowered until the ionization time is just at the maximum value, or switching between the maximum value and just below it. This gives the software the full range of ionization time to adjust for any additional ions injected into the trap and

minimizes the contribution from background ions. This method was used to set the ion source pressure and successfully detect 100 fg of a decafluorobenzophenone standard with a signal-to-noise of 13 on th GCQ.

The emission current is directly proportional to the number of electrons emitted from the filament. Thus, the number of ions generated in the source should be directly proportional to the emission current. Figure 2-17 confirms this trend. Figure 2-18 shows the signal-to-noise ratio decreasing for positive CI ions of decafluorobenzophenone with increasing emission current. This trend is not always observed. For ions with relatively high signal-to-noise at low emission currents, the signal-to-noise was not observed to change significantly with an increase in emission current.

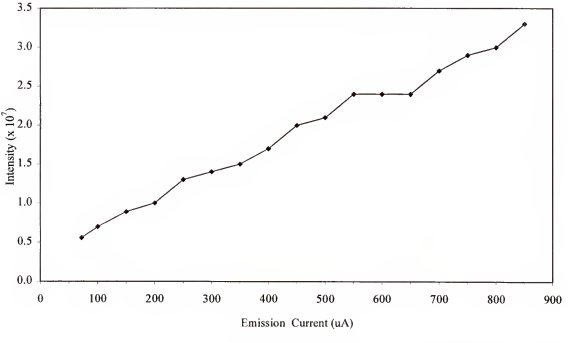

Figure 2-17: Intensity versus emission current for negative ions of FC43 acquired in SIM mode at 300 mTorr source pressure and 100 eV electron energy.

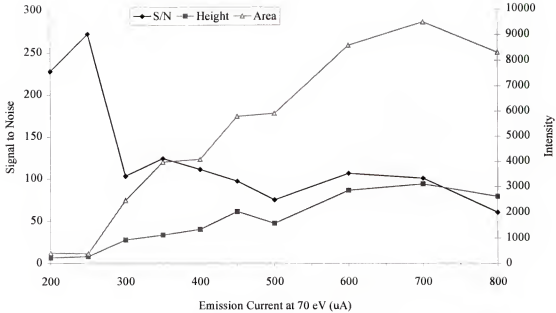

Figure 2-18: Peak intensity, area, and signal-to-noise ratio of m/z 363 ions versus emission current for single 100 pg injections of decaflourobenzophenone in positive CI.

Calculating Reaction Time

When studying reactions that take place in the ion trap it is often necessary to know the amount of time that the ions have to react with the neutrals. For example, in full scan mode the ions are injected into the trap and immediately have the opportunity to react with neutrals present up until the ions are scanned out of the trap. Aside from knowing the ionization time, no other time events are known without studying the instrument source code. Table 2-4 lists important times for the events that can contribute to the total reaction time in the various scan modes. In full scan, half of the ionization time is used to account for the average residence time for ions arriving in the trap at the beginning and end of the ion injection. In SIM and MS/MS modes, the reaction time

begins after the isolation event because any previously generated ion/molecule reaction products are ejected during the isolation step.

Table 2-4: Reaction times for various scan modes.

Full Scan	**Time (ms)**
Ionization time	X
Post-ionization time	3
Ramp time	1
Multiplier warm-up time	2
Backstep time	1.08
Scan time (mass – first mass) × 0.180 ms/amu	Z
Total Reaction Time	X/2 + 7.08 + Z

MS/MS	**Time (ms)**
Ramptime	1
Cooltime	1
Pulse time (SweetP only)	P
Tickletime	Y
Ramp time	1
Multiplier warm-up time	2
Backstep time	1.08
Scan time (mass – first mass) × 0.180 ms/amu	Z
Total Reaction Time*	P + Y+ 6.08 + Z

SIM	**Time (ms)**
Multiplier warm-up time	2
Backstep time	1.08
Scan time (mass – first mass) × 0.180 ms/amu	Z
Total Reaction Time	3.08 + Z

*The total reaction time will be (P-0.7) + Y + 4.08 + Z if the neutral reactant is admitted to the ion trap through the pulsed valve.

The time for the scan out of masses up to the reactant ion can be significant. For example, it takes 19.26 ms to scan from m/z 40 to m/z 147 at 180 μs/amu. If the scan rate is changed to 90 μs/amu, this time is cut in half.

Calculation of Number of Ions in the QITMS

When studying the kinetics of ion/molecule reactions, it is useful to know the number of ions actually in the ion trap. In the GCQ, automatic gain control (AGC) is used to control the number of ions injected into the ion trap by adjusting the ionization time based upon total ion counts (TIC) measurements from a pre-scan ionization time (usually 2 ms). The equation for AGC in the QITMS is:

Ionization time = Pre-scan Ionization Time × AGC Target / Pre-scan TIC (2-8)

The AGC target is directly proportional to the number of ions in the QITMS during the analytical scan. Equation 2-9 was adapted from a calculation done by Jae Schwartz at Finnigan. It shows the calculation for the number of ions in the ion trap for an AGC target of 50 (5.0×10^8 counts), a detector gain of 3.5×10^5, a sample rate of 15 samples/amu, and a scan rate of 180 μs/amu.

$$5.0\times10^8\,\text{counts}\times\left(\frac{5.0\times10^{-6}\,e^-\cdot\text{A}}{2.38\times10^8\,\text{counts}}\right)\times\left(\frac{1\,\text{ion}}{3.5\times10^5\,e^-}\right)\times\left(\frac{1\,\text{e}^-}{1.6021\times10^{-19}\,\text{A}\cdot\text{s}}\right)\times\left(\frac{180\times10^{-6}\,\text{s/amu}}{15\,\text{samples/amu}}\right)=2248\,\frac{\text{ions}}{\text{samples}}\,\text{detected}\times2\approx4500\,\text{ions in the ion trap} \quad (2\text{-}9)$$

The (e^-A/counts) term represents the response of the analog-to-digital converter. The ions detected are multiplied by 2 because the assumption is made that only half of the ions exit the QIT through the exit endcap and the other half exit through the entrance endcap.

Conclusions

Chemical ionization with ion injection into ion traps creates many exciting possibilities for studying gas-phase chemistry and for mass spectrometry. The parameters

described in this chapter reflect the major parameters necessary for adjustment in operation of these ion injection instruments. The value of discussing these parameters is to become familiar with sensitive ionization methods and sensitive detection. The QITMS is more sensitive than many mass spectrometers. It must be understood that with ion injection, the QITMS is still not a beam instrument and has a limit to the number of ions that can be placed inside. In some cases to obtain the best signal-to-noise less ion intensity from the source is best. Ion injection QITMS instruments are unlike internal ionization QITMS instruments, where high pressure CI was not an option and low pressures with long reaction times were used to obtain CI products. A high pressure external source creates an abundance of ions in a relatively short time. The QITMS still holds the same number of ions regardless of where they were produced; therefore, the QITMS with ion injection does not require the source to operate at maximum efficiency when maximum efficiency generates too many ions.

CHAPTER 3
CHIRAL ION/MOLECULE REACTIONS

General Overview

Fales and Wright (1977) first reported chiral discrimination in gas-phase ion/molecule reactions in 1977. They observed unequal abundance of homochiral and heterochiral dimer formation for protonated dialkyl tartrates in CI mass spectrometry. Since this discovery, others have confirmed these chirality effects in dimer formation in the gas phase and have used semi-empirical calculations to explain differences in association energies of these complexes (Nikolaev et al., 1988; Honovich et al., 1992; Winkler et al., 1994). Furthermore, chiral discrimination has been shown to occur in other areas of mass spectrometry, such as chiral host-guest complexation between chiral crown ethers and chiral ammonium cations in fast atom bombardment mass spectrometry (Pocsfalvi et al., 1996; Sawada et al., 1993).

This chapter discusses two different types of chiral ion/molecule reactions investigated in the SweetP instrument to determine if chiral discrimination can be observed in selective reactions within the QITMS. The first reactions studied were Diels-Alder association reactions involving reagent ions formed from chiral reagents and chiral molecules. The second set of reactions studied were condensation ion/molecule reactions involving isopinocampheol and phenylethylamine enantiomers which had been reported

to exhibit chiral discrimination within CI mass spectrometry and MS/MS (Sellier et al., 1994).

Diels-Alder Ion/Molecule Reactions

Background

The Diels-Alder reaction (1,4-cycloaddition of dienes) was discovered in 1928 by Otto Diels and Kurt Alder (Solomons, 1988). It was of such great use in organic synthesis that Diels and Alder were awarded the Nobel Prize for Chemistry in 1950. The Diels-Alder reaction involves formation of a cyclic product between a 4π-electron system (diene) and a 2π-electron system (dienophile) such as the example in Figure 3-1(Solomons, 1988). In this reaction, π and σ bonds are interconverted in a single concerted step to form a closed ring. The stereochemistry of the diene is usually retained in the product. Stereospecificity has been seen in the study of retro-Diels-Alder fragmentation of cyclic gas-phase ions studied by MS/MS (Denekamp et al., 1996).

Figure 3-1: Example of a simple Diels-Alder cycloaddition reaction.

In solution, the reactivity of normal Diels-Alder reactions is determined by the energy gap between the highest occupied molecular orbital (HOMO) of the diene and the lowest unoccupied molecular orbital (LUMO) of the dienophile. Lu et al. (1995) have

reported that Diels-Alder ion/molecule reactions between protonated and methylated ketone ions and butadiene are favorable, in general, when the calculated energy gap between the ion LUMO and the neutral HOMO is less than 3 eV.

The Diels-Alder reactions studied in this lab involved reactions between acylium ions (dienophiles) and neutral dienes. Diels-Alder ion/molecule reactions involving acylium ions and neutral dienes have been studied within a pentaquadrupole mass spectrometer and QITMS in the Cooks group (Eberlin and Cooks, 1993; Soni et al., 1995). The cycloaddition reaction of the mass-isolated benzoyl cation (acylium ion from acetophenone) at m/z 105 and neutral 2-methyl-1,3-butadiene (isoprene, mass 68) was duplicated on the SweetP instrument to determine the feasibility of the mass-selective experiment in the ion injection instrument. The product at m/z 173 (figure 3-2) was

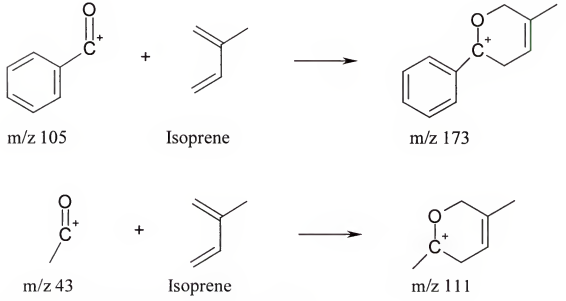

Figure 3-2: Acylium ion reactions with isoprene.

readily observed. Also, the methyl acylium ion (acylium ion from methyl acetate) at m/z 43 was mass-isolated and reacted with isoprene pulsed into the SweetP QITMS and found to form an abundant cycloaddition product at m/z 111.

Choosing Chiral Reactants

For this study chiral reagents were chosen with properties similar to previously studied acylium ions and dienes for Diels-Alder reactions. The HOMO-LUMO energy gaps were then calculated (see below) to predict the reactivity of the cycloaddition before obtaining the reactants. The acylium ions of (R) and (S)-methyl-2-chloropropionate (Figure 3-3) were chosen as possible chiral dieneophiles for ion/molecule reactions because of the proximity of the chiral center to the acylium bond and the commercial availability of the molecules. Acetonides (Figure 3-3) were chosen as possible chiral dienes for this study because they could be synthesized from diols prepared within the department by microbial dioxygenation of aromatics by *Pseudomonas putida* (Hudlicky and Boros, 1993). The microbial synthesis should produce only one enantiomer. The isopropylidine protecting group and ring structure should keep the stereochemistry of these enantiomers fixed during ion/molecule reactions.

Semi-empirical calculations were used to determine the orbital energies for the methyl-2-chloropropionate acylium ion and for the acetonides with different functional groups. The HOMO-LUMO energy gaps were then used to predict their reactivity towards cycloaddition. Orbital energies were obtained by using an MM+ Polak-Rabiere geometry optimization and extended-Hückel theory (EHT) single point energy calculation on each species and then recording orbital energy calculations within

HyperChem Lite (HyperCube, Waterloo, Ontario). Table 3-1 lists the results of these calculations. From the data it appears that all of the reactions should be favorable, since the energy gaps are all less than 3 eV. The bromoacetonide, having the lowest calculated energy gap of 1.75 eV, was chosen as the neutral reagent for further calculations and

Diene = Chiral Compound with Isopropylidine Protecting Group

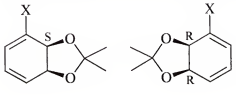

X =	MW =
Br	230, 232
Cl	186, 188
CH_3	166
CF_3	220
$CHCH_2$	178

Dienophile = Acylium Ion from a Chiral Ester

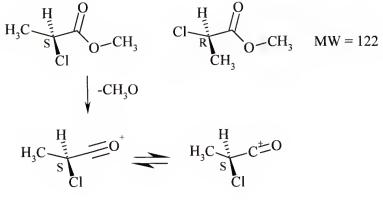

MW = 122

Diels-Alder Cycloaddition

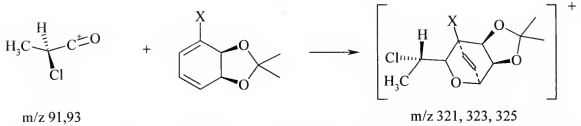

m/z 91,93

m/z 321, 323, 325

Figure 3-3: Chiral Diels-Alder ion/molecule reaction involving methyl-2-chloropropionate acylium ions and acetonides of cyclohexadiene diols.

study with the instrument. Single point energy calculations were performed using HyperChem Lite on possible reaction products for the chiral acylium ion reaction with bromoacetonides. Table 3-2 presents results of these calculations.

Table 3-1: HyperChem orbital calculations for ion LUMO – neutral HOMO energy gaps.

Ion:	LUMO (eV)
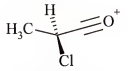	-9.89152

Molecule:	HOMO (eV)	Energy Gap (eV)
X = Br	-11.64054	1.749024
X = Cl	-11.95058	2.059064
X = CH3	-11.94444	2.052924
X = CF3	-12.06346	2.171944
X = CH2CH3	-11.76892	1.877404
Isoprene	-12.26714	2.375624

Table 3-2: Single point energy calculations for possible cycloaddition reaction products.

Reaction	Side	O vs. CBr	EHT E (kcal/mol)	d(kcal/mol)	d(eV)
S + R,R	FRONT	PROXIMAL	-39739.714310	0.29858	0.01295
R + S,S	FRONT	PROXIMAL	-39740.012887	1.33730	0.05799
S + S,S	FRONT	PROXIMAL	-39741.350185	0.15122	0.00656
R + R,R	FRONT	PROXIMAL	-39741.501408	0.68816	0.02984
S + R,R	FRONT	DISTAL	-39742.189569	0.14786	0.00641
R + R,R	FRONT	DISTAL	-39742.337430	0.05794	0.00251
R + S,S	FRONT	DISTAL	-39742.395369	0.06210	0.00269
S + S,S	FRONT	DISTAL	-39742.457472	5.52480	0.23958
S + R,R	BACK	PROXIMAL	-39747.982269	0.03301	0.00143
S + S,S	BACK	PROXIMAL	-39748.015281	0.15044	0.00652
R + R,R	BACK	PROXIMAL	-39748.165723	0.12439	0.00539
R + S,S	BACK	PROXIMAL	-39748.290111	2.36199	0.10243
R + S,S	BACK	DISTAL	-39750.652104	0.19225	0.00834
S + R,R	BACK	DISTAL	-39750.844357	0.08878	0.00385
S + S,S	BACK	DISTAL	-39750.933136	0.13445	0.00583
R + R,R	BACK	DISTAL	-39751.067586		

For the purpose of describing the products, the front-side reaction refers to ring formation on the side of the acetonide facing the cis-diol bonds. The O versus CBr refers to whether the acylium oxygen is attached to the bromide carbon of the acteonide (proximal), or separated by the acylium carbon (distal). The calculated differences in energies for the lowest energy conformations were less than 0.3 kcal/mol, which suggested that differences in reactivity would be difficult to observe based solely on the energy of the products.

Experimental

All chiral ion/molecule reactions were performed on the SweetP instrument with the Finnigan ITS 40 QIT and GCQ ion source. The (R)- and (S)-methyl-2-chloropropionate were purchased from Aldrich. Vapors from the neat reagents were admitted into the ion source via a Granville-Philips Series 203 variable leak valve (setting ~ 4) to yield ion gauge pressures of 2×10^{-6} to 5×10^{-6} Torr. Isoprene was obtained from the Katritzky group (UF) and (S,S)-bromoacetonide was obtained from the Hudlicky group (UF). These neat reagents were admitted into the QITMS through a General Valve (Fairfield, NJ) Series 9 pulsed valve (orifice diameter 0.006") plumbed directly into the trap. The pulse duration was typically 1-2.5 ms (a minimum of approximately 700 μs is required for the valve to open). There were no observable changes in ion gauge pressure for these pulses.

The appropriate ionization method for most intense formation of the mass-selected acylium ions of methyl-2-chloropropionate was determined on both the GCQ and SweetP instruments. EI of methyl-chloropropionate produced a large $[M\text{-}Cl]^+$

fragment ion as base peak, leaving insufficient acylium ions $[M\text{-}CH_3O]^+$ for reagent ions. Methane CI produced an abundant $[M+H]^+$ ion as base peak. Performing CID in the trap (at 1.1 $V_{p\text{-}p}$ resonant excitation amplitude) on the $[M+H]^+$ ions produced the acylium ions as base peak. The acylium ions (m/z 91 & m/z 93) used for the ion/molecule reactions were therefore produced via CID of the $[M+H]^+$ ions and isolated prior to introduction of the neutral. Isolation of the acylium ions in the QITMS was accomplished by varying RF and DC on the ring electrode similar to two-step isolation (Yates et al., 1991).

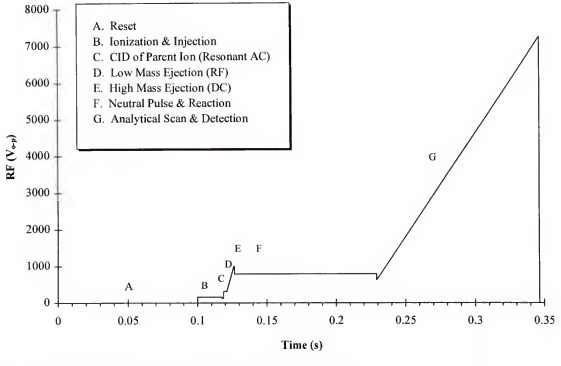

Figure 3-4: Time diagram showing RF versus time for the reaction sequence.

The methyl-chloropropionate acylium ions were tested for reaction with isoprene in order to optimize the reaction scan function on the ITS 40 data system prior to performing the experiment with bromoacetonide neutral. Figure 3-4 shows the time

diagram for the experiment, plotting RF amplitude versus time for a single scan. The resulting plot for the reaction time study of the reaction between isoprene and methyl-2-chloropropionate acylium ions is shown in Figure 3-5. The reaction time (reagent pulse to the start of the scan) was varied from 0.3-100 ms. From this data, 30 ms was chosen for the initial reaction time for the chiral reaction with bromoacetonide. The actual reaction time, as discussed in Chapter 2, also includes a portion of the pulse time and the time of the analytical scan up until the reactant ions are ejected from the trap.

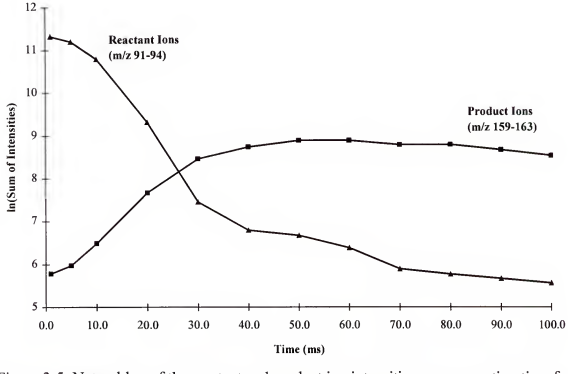

Figure 3-5: Natural log of the reactant and product ion intensities versus reaction time for the reaction of a mixture of (R)– and (S)-methyl-2-chloropropionate acylium ions with isoprene.

For the chiral reaction, bromoacetonide was placed within a sample vial attached to the pulsed valve on the QITMS. The sample vial was heated in a water bath between

40 and 80°C to raise the vapor pressure of the acetonide. The pulse duration for admitting the bromoacetonide into the ion trap for reaction was determined by injecting methane positive CI reagent ions and allowing them to react with pulses of the acetonide. It was determined that a 1.5 ms pulse with a 30 ms reaction time was sufficient to obtain well resolved $[M+H]^+$ ions (m/z 231, 233) of the acetonides from internal CI within the QIT in SweetP. Pulses of 1.5 ms to 2.5 ms were used for the reaction with the chiral acylium ions.

Results

Ions of the correct m/z (m/z 321, m/z 323, and m/z 325) for the Diels-Alder adduct were observed at less than 12% relative intensity (Figure 3-6). The intensities of these ions were not reproducible, and their structures could not be confirmed by MS/MS due to their low abundance. Chiral selectivity in the reaction was not observed; that is, reactions between the bromoacetonide sample and the acylium ion of each enantiomer of the chloropropionates produced the same product ions. The relative abundances of each product and fragment could not be compared due to low intensity and irreproducibility.

The fact that the product showed isotopic peaks including the M+4 isotope reveals that the product ion did retain both the bromine atom and the chlorine atom. The correct isotopic pattern for a single bromine and a single chlorine is 1:1.3:0.3. The M+2 and M+4 isotopes were most likely less intense than expected because the resonant excitation frequency used to fragment the $[M+H]^+$ methyl-2-chloropropionate ions (m/z 123, 125) and form the acylium reagent ions (m/z 91, 93) was tuned for optimum fragmentation of

the ^{35}Cl isotope ion at m/z 123. This would produce more m/z 91 reagent ions than m/z 93 reagent ions.

Product ions produced at lower masses in the spectra could result from fragmentation of the ion/molecule product ion or from charge exchange to form acetonide ions (m/z 230, 232) and subsequent fragmentation. One fragment cluster, appearing at m/z 173 and 175, appeared to be due to fragmentation of the acetonide ions to form bromophenol ions. The isotope pattern of approximately 1:1 (M:M+2) indicates the presence of a single bromine. To be certain these peaks were not the result of reactions with other neutrals in the trap, the reaction was repeated with a 100 ms reaction table with the pulsed valve off. No product ions were formed from the acylium ions in this case. Perhaps, because the HOMO-LUMO energy gap was so low, the reaction was too energetic; however, this does not match the trends reported by Lu et al. (1995). The lowest energy gap they reported was 1.73 eV for the reaction between protonated benzoquinone and butadiene. This reaction also had the highest yield, 50%.

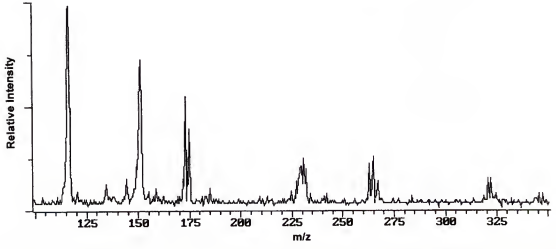

Figure 3-6: Reaction of a racemic mixture of methyl-2-chloropropionate acylium ions with bromoacetonide.

Conclusions

The low abundance of the chiral Diels-Alder product and the extensive fragmentation observed in the product spectra led to the conclusion that the reaction was more energetic than anticipated. This was based on the results of earlier Diels-Alder reactions with acylium ions (Figure 2-3) which showed intense Diels-Alder adducts and showed almost no fragmentation. The acetonide reactions required a great deal of time to set up in the ITS 40 software and to optimize instrument parameters, including adjusting neutral pressure (wasting valuable reagents prepared by another group in the process). The decision was made to try ion/molecule reactions (such as the phenylethylamine/isopinocampheol reactions described below) which were reported to show enantioselectivity on other types of instruments, rather than repeat the Diels-Alder reactions with other acetonides.

Isopinocampheol Reactions with Phenylethylamine

Chiral ion/molecule reactions between isopinocampheol and phenylethylamine in the QIT and in the external ion source were performed and the results compared to data (acquired on Nermag R 10-10C and Nermag R 30-10 single and triple quadrupole mass spectrometers) that had been reported by Sellier et al. (1994) to demonstrate enantioselectivity. By analyzing solid isopinocampheol on a direct exposure probe under CI using (R)- and (S)-phenylethylamine as chiral reagent gases, Sellier et al. reported different ion peak intensities for the $[M\text{-}H_20\text{+phenylethylamine+H}]^+$ (m/z 258) and $[M\text{+phenylethylamine+H}]^+$ (m/z 276) ions for (+) and (-) isopinocampheol. They also

reported that MS/MS of these ions could be used to differentiate enantiomers. The enantiomeric reactant molecules are pictured below in Figure 3-7.

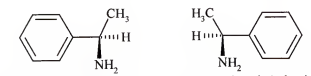

(R)-(+)-1-phenylethylamine (S)-(-)-1-phenylethylamine MW=121

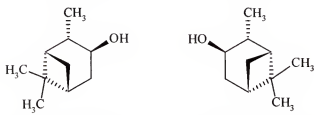

(+)-isopinocampheol (-)-isopinocampheol MW = 154

Figure 3-7: Enantiomers used for ion/molecule reactions.

This section describes the study of phenylethylamine CI in the external ion source and ion/molecule reactions in the ion trap for the purpose of reproducing these enantioselective reactions in the SweetP instrument. If differences could be seen between ions from different enantiomers in the source, selective ion/molecule reactions in the QIT should be able to enhance the differences. Being able to clearly demonstrate chiral selectivity in MS/MS of CI products would be useful evidence that the CI ionization process may not destroy the stereochemistry of (i.e., racemize) the starting molecule upon ionization, and that energetic differences are retained in the reaction products.

Experimental

All data presented here was acquired on the SweetP instrument with the GCQ ion source and QIT. Relative peak intensities of the products of reactions in the trap were obtained by averaging results for six experiments, each with an average of 100 spectra.

Ion intensity data for the source CI reactions were taken from peak intensities averaged for ten individual experiments. Each experiment included an average of 300 individual spectra.

Optically pure samples of phenylethylamine enantiomers (≥97%) and isopinocampheol (≥98%) were purchased from Fluka (Milwaukee, WI). They were used without further testing or purification.

Isopinocampheol neutral vapor was admitted into the trap through 1/16" stainless tubing or by pulsed valve (0.6 mg added to a sample vial attached to the pulsed valve). The pressure change due to admitting isopinocampheol into the ion trap was not noticeable on the ion gauge. The uncorrected ion gauge reading in the trap chamber was 3×10^{-6} Torr with trapping helium.

For GC/MS, 1.5 ug of isopinocampheol in acetone were injected (splitless) onto a DB-5 capillary column (11m long, 0.25 mm I.D.). Phenylethylamine was leaked into the ion source (CI ion volume) through a 1/16" stainless tubing restrictor to achieve an ion gauge partial pressure of 2.4×10^{-5} Torr. The source pressure was approximately 30 mTorr, measured by capacitance manometer. The transfer line temperature was set to 275°C and the ion source temperature was 200 °C.

Methane and isobutane CI of phenylethylamine produced $[M+H]^+$ ions (m/z 122) with a relative intensity 8% of the m/z 105 base peak $[M+H\text{-}NH_3]^+$, while ammonia CI produced only 1% $[M+H]^+$ ions. Self-CI was found to produce the most intensity of $[M+H]^+$ ions and was used to form m/z 122 for ion/molecule reactions in the QITMS.

The ionization time was fixed at 5 ms for MS/MS studies of ions formed in the QITMS by ion molecule reactions. For all other MS/MS and full scan studies the ionization time was adjusted by the instrument control software with a target value of 50. The CID event in MS/MS experiments was set to 15 ms with resonant excitation at 0.35 V_{pp}. The reaction time for the formation of MS^3 parent ions was 30 ms. The reaction time for the ion/molecule reaction between phenylethylamine m/z 122 ions and neutral isopinocampheol was 3000 ms. The neutral pulse was 1.4 ms for these reactions.

Results

Ions which formed the product ions at m/z 276 and m/z 258 were found by isolating ions in 20 m/z wide ranges and allowing them to react with neutral isopinocampheol in the trap. Once a 20 m/z range of ions was found to produce the selected products, the mass range of ions isolated was decreased until the specific reactant ions were located. Ions forming 276 were m/z 155 (isopinocampheol $[M+H]^+$) and m/z 122 (phenylethylamine $[M+H]^+$). Ions forming 258 were 105 (phenylethylamine $[M-NH_2]^+$) and m/z 137 (isopinocampheol $[M+H-H_2O]^+$).

Some chiral differentiation may be possible from the ion intensities of ion/molecule reaction products formed by mass-selected reactions with m/z 122 ions in the QITMS (Table 3-3). It is more probable, however, that inability to control the neutral pressure accounts for different ion intensities of ions formed in the QITMS. The neutral isopinocampheol pressure for the data presented in Table 3-3 was difficult to keep constant, because of temperature fluctuations in the pulse valve and plumbing during the experiment. For example, when adjusting the vapor pressure of the isopinocampheol in

the QIT, the m/z 258 ion was as much as 32% of the ion at m/z 137, and the ion at m/z 276 was as much as 329% of m/z 137 (isopinocampheol $[M+H-H_2O]^+$). This is a huge variation from the values in Table 3-3 acquired with fairly stable reagent pressure. The differentiation in the m/z 258 ion intensities in Table 3-3 could be due to the amount of neutral phenylethylamine present in the QITMS from the background as well as slight changes in temperature and vapor pressure of the isopinocampheol neutral from enantiomer to enantiomer (the data were not acquired in the same day, because the phenylethylamine enantiomers had to be purged from the plumbing and source). The pulsed valve was located inside the vacuum manifold for this experiment and had difficulty dissipating heat. It was later discovered that moving the pulsed valve outside of the vacuum chamber allowed much better cooling of the solenoid.

Table 3-3: Ion intensities relative to m/z 137 for products of the (+)-isopinocampheol ion/molecule reaction with mass-isolated phenylethylamine m/z 122 ions in the QITMS.

	m/z 258			m/z 276		
Reagent	%	Std. dev.	ref. %*	%	std. dev.	ref. %*
R(+)-1-phenylethylamine	4.15	0.55	19	21.28	3.47	9
S(-)-1-phenylethylamine	1.91	0.69	5	22.44	2.01	7

*Source: Sellier et al., 1994.

Chiral discrimination was not observed in the reactions from the external ion source (Table 3-4). The reported values from Sellier et al. do not include statistical data, so it is difficult to make judgements based upon these results. It was not possible to duplicate their method of sample introduction into the source. They placed 60 μg of neutral isopinocampheol on a direct exposure probe tip and inserted it into their CI source. An attempt to reproduce this method of introduction on the SweetP instrument failed because most of the sample was lost in transit from atmosphere, through the probe

lock, and into the ion source. The GC/MS results obtained in this lab (Table 3-4) should be more reproducible because known sample amounts were admitted into the ion source through the GC column for all reactions.

Table 3-4: Ion intensities relative to m/z 137 for CI mass spectra of isopinocampheols with phenylethylamine as a reagent gas in the external ion source.

	m/z 258			m/z 276		
Reactants	%	std. dev.	ref. %*	%	std. dev.	ref. %*
R(+)-1-phenylethylamine + (+)-isopinocampheol	10.95	1.19	19	2.22	2.12	9
R(+)-1-phenylethylamine + (-)-isopinocampheol	10.87	1.83	2	2.70	2.04	1
S(-)-1-phenylethylamine + (+)-isopinocampheol	8.47	1.54	5	0.16	0.19	7
S(-)-1-phenylethylamine + (-)-isopinocampheol	11.52	2.20	4	0.79	1.13	5

*Source: Sellier et al., 1994.

The MS/MS spectra of the product ions formed by source CI (Figures 3-8 and 3-9) did not significantly differ from the MS/MS spectra of ions generated via ion/molecule reactions within the QIT involving all phenylethylamine reagent ions, which will be discussed below. Figure 3-10 shows proposed structures and pathways for the ions observed in these spectra. Ion/molecule reaction product ions generated from selected reagent ions and neutrals did, however, reflect the different starting reagents in their MS/MS spectra. For example, m/z 276 formed in the ion source produced a fragment ion at m/z 155 (isopinocampheol $[M+H]^+$). The m/z 155 fragment was only seen in the MS/MS spectra of m/z 276 that was generated in the QIT by m/z 155 reagent ions (protonated isopinocampheol from a previous ion/molecule reaction). The MS/MS spectra of m/z 276 generated from protonated phenylethylamine ions (m/z 122), in contrast, showed no fragments at m/z 155. Figure 3-11 shows the full profile scan of products formed from all phenylethylamine ions and isopinocampheol leaked into the ion

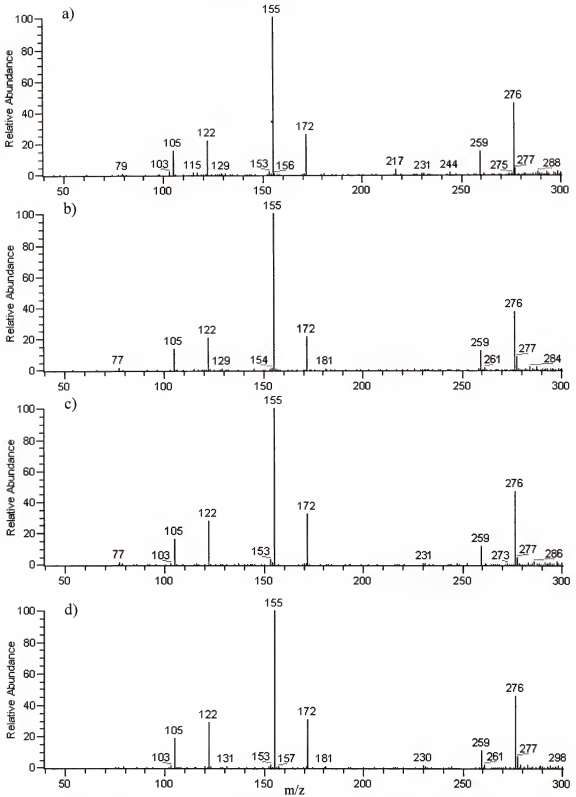

Figure 3-8: MS/MS of m/z 276 from phenylethylamine-CI (Pea-CI) in the ion source. a) (R)- (+)-Pea-CI of (+)-isopinocampheol; b) (R)- (+)-Pea-CI of (-)-isopinocampheol; c) (S)-(-)-Pea-CI of (+)-isopinocampheol; d) (S)-(-)-Pea-CI of (-)-isopinocampheol.

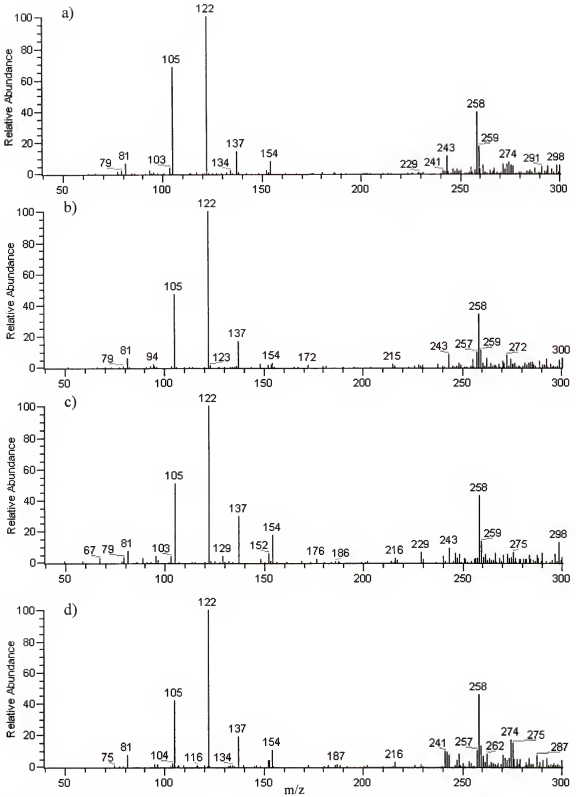

Figure 3-9: MS/MS of m/z 258 from phenylethylamine-CI (Pea-CI) in the ion source. a) (R)- (+)-Pea-CI of (+)-isopinocampheol; b) (R)- (+)-Pea-CI of (-)-isopinocampheol; c) (S)-(-)-Pea-CI of (+)-isopinocampheol; d) (S)-(-)-Pea-CI of (-)-isopinocampheol.

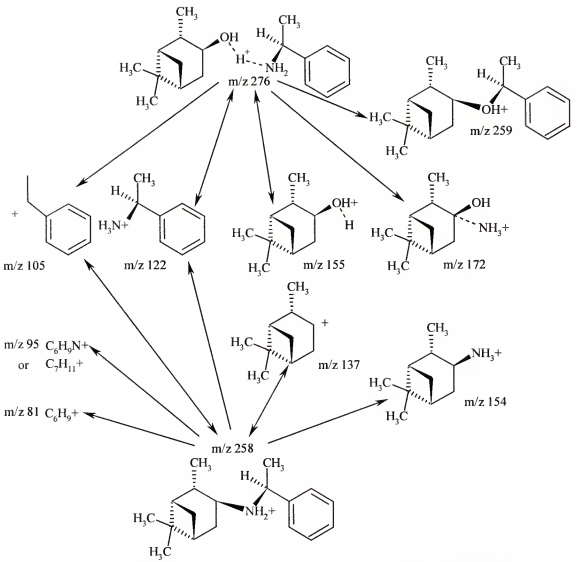

Figure 3-10: Proposed structures of ions observed in MS/MS of m/z 276 and m/z 258. Double arrows represent ion/molecule reaction pathways to the ion of higher m/z, as well as fragmentation pathways.

trap. These product ions were used to form other ions studied by MS/MS in Figure 3-12, mentioned above and discussed again below.

The fragment ions from the product ions generated in the source appear to result from fragmentation of both collisionally stabilized association and condensation complexes. The ions at m/z 155 and m/z 122 in the product spectra for MS/MS of m/z

276 are the result of fragmentation of an association complex, since these are the same ions that form m/z 276. The ions at m/z 137 appearing in the MS/MS spectra of m/z 276 result from condensation reactions, since the m/z 137 ions do not form the m/z 276 products (Figure 3-10).

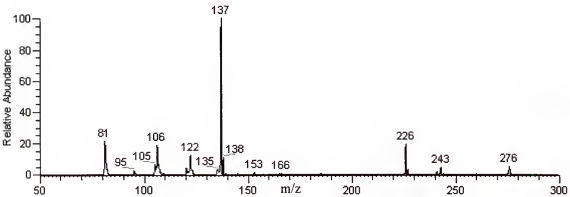

Figure 3-11: Full profile scan of products formed from reaction of all (R)-(+)-phenylethylamine ions and (+)-isopinocampheol leaked into the ion trap.

There is evidence that some neutral phenylethylamine diffuses into the ion trap from the ion source in the SweetP instrument. Ions at m/z 243 (proton bound dimers of phenylethylamine) appear in most spectra. Also, the observed reaction in which m/z 137 forms m/z 258 (Figure 3-12a), is not possible without neutral phenylethylamine in the trap. The m/z 258 ion is only produced by m/z 137 plus neutral phenylethylamine, or by m/z 105 plus neutral mass 153 (which is the neutral loss in the m/z 258 fragmentation to form m/z 105). The only other reaction that forms neutral phenylethylamine (the fragmentation of m/z 276 to m/z 155) is not seen in full scan. The low ion intensities for m/z 258 formed in the QIT (Table 3-3) compared to the ion intensities in Table 3-4 also reveal that the formation of m/z 258 is much more favorable in the source where both phenylethylamine and isopinocampheol neutrals are present in abundance.

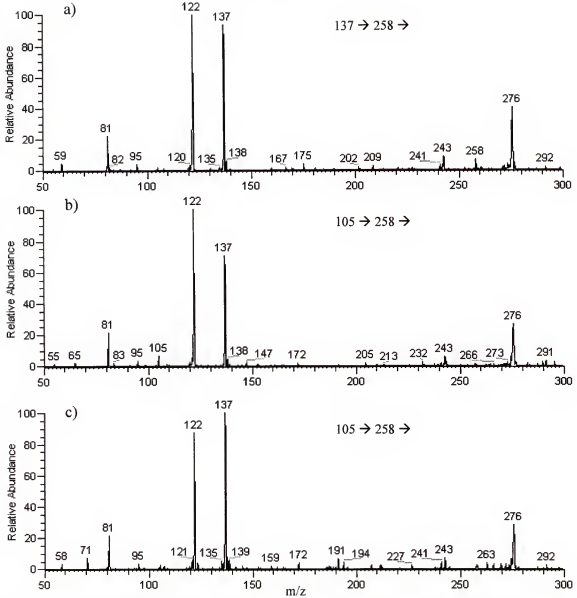

Figure 3-12: MS/MS/MS product spectra of isolated m/z 258 formed by ion/molecule reactions in the QIT between isolated fragment ions and isopinocampheol. a) Ion at m/z 137 from (R)-(+)-phenylethylamine ions and (-)-isopinocampheol in the QIT, isolated and reacted with neutral (-)-isopinocampheol to form m/z 258; b) Ion at m/z 105 from (R)-(+)-phenylethylamine ions and (-)-isopinocampheol in the QIT, isolated and reacted with neutral (-)-isopinocampheol to form m/z 258; c) Ion at m/z 105 from (R)- (+)-phenylethylamine ions and (+)-isopinocampheol in the QIT, isolated and reacted with neutral (+)-isopinocampheol to form m/z 258.

The MS/MS spectra of reaction products from (R)-phenylethylamine ions plus (-)-isopinocampheol and (R)-phenylethylamine plus (+)-isopinocampheol (Figure 3-12b-c)

reveal the same fragmentation trends that Sellier et al. report. The m/z 137 intensity increases relative to other fragments for the (R)-phenylethylamine plus (+)-isopinocampheol reaction and the m/z 105 intensity increases for the (R)-phenylethylamine plus (-)-isopinocampheol reaction.

Conclusions

The ability to mass-select reactant ions and produce ion/molecule reaction products in the SweetP instrument has been shown. The reactions, while more selective within the QIT than in the ion source, were not able to conclusively demonstrate enhanced chiral selectivity over other reported results for the interactions between phenylethylamine and isopinocampheol (Sellier et al., 1994). The MS/MS data for m/z 258 ions formed in the QIT (Figure 3-12) may allow differentiation between enantiomers of isopinocampheol, although this seems unrealistic because the m/z 258 ions were formed from ion/molecule reactions with achiral m/z 105 fragment ions.

Fluctuations in neutral vapor pressure in the trap were observed to cause large shifts in ion intensities, as one would expect. It is possible that the deviations in peak intensities reported in Table 3-3 are due to vapor pressure fluctuations and not chiral effects. Racemates are known to have different vapor pressures and melting points from their pure enantiomers (Fales and Wright, 1977). If one of the pure enantiomer samples in this study were to have racemized to a different extent than the other enantiomer, it could have a different vapor pressure in the instrument and throw off the ion intensities.

It may be useful to attempt these reactions again with a chiral GC column plumbed into the ion trap and attempt to introduce the isopinocampheol reagents in small

reproducible injections into the ion trap. This would require modifying the conductance of the trap to accommodate the increased helium flow into the trap.

The results presented in Table 3-4 reveal that chiral differentiation is not observed for isopinocampheol enantiomers with the enantiomers of phenylethylamine as reagent gases in the external ion source. These data do not rule out or corroborate the possibility for chiral selectivity in gas-phase reactions in the SweetP instrument.

CHAPTER 4
ION/MOLECULE REACTIONS WITH WATER

Introduction

This chapter reviews ion/molecule reactions with water studied on the GCQ QITMS. The partial pressure of water within the manifold of an operational GCQ is approximately 1 to $3x10^{-7}$ Torr depending upon the vacuum pump used. This water is largely due to outgassing from the GCQ manifold and o-rings, and the water introduced with the helium entering the GCQ, as discovered by experiments performed at Finnigan (Austin,TX). Water is replenished by low levels of water in the helium entering the chamber from two entry points: via the GC through the source, and directly into the ion trap via a fused silica capillary restrictor, discussed in Chapter 2.

Any amount of water that enters the ion trap volume may react with the ions trapped inside. The extent of these reactions, for a given analyte, is a function both of the amount of water present and the time an ion is contained. Water adducts, proton abstraction from molecular ions, and condensation reactions are common. For example, methylene chloride and chloromethane molecular ions ($CH_2Cl_2^+$ and CH_3Cl^+) protonate water to form H_3O^+ and a neutral chlorinated radical, causing loss in sensitivity for the molecular ions (as shown below in methylene chroride spectra). Fragment ions of trimethylsilyl (TMS) derivatives of organic acids react with water to exchange a methyl group with a hydroxyl group, increasing the fragment ion m/z by 2 (as shown below).

Perfluorotributylamine m/z 219 ions, $CF_3(CF_2)_3^+$, adduct with water and loose 2HF to form m/z 197, $CF_3(CF_2)_2CO^+$. Several of these ion/molecule reactions with water were studied to pick a hygrometer useful for spectrally determining the amount of water present in the QITMS.

Water reactions with TMS derivatives were chosen as a hygrometer because the chromatography was simple and useful for quantitatively reproducible reactions, the product and reactant ions were in a similar mass range, and time-dependent behavior was easy to observe. In addition, the TMS-water reaction is first-order with respect to water pressure, and first-order with respect to number of reagent ions in the ion trap, so the rate is directly proportional to the water concentration in the ion trap. (Throughout this chapter, the term ion concentration is often used synonymously with the number of ions trapped in the QIT).

In the course of studying the TMS derivatives, the QIT trapping (buffer gas) helium was found to be the major source of water for ion/molecule reactions in the ion trap. Trap conductance calculations (below) show that the water vapor partial pressure within the trap is ten times higher than the partial pressure of water measured outside the trap due to other sources besides the buffer helium. By drying the buffer helium with liquid nitrogen, a molecular sieve, or a Peltier trap, the water reactions were reduced considerably in the ion trap. This chapter describes some of the reactions with water that occur in the ion trap and does not address the measures taken to reduce the water in the trapping helium.

The spectra in Figure 4-1 demonstrate the differences between QITMS spectra and reference spectra resulting from water reactions. The first spectrum is the NIST

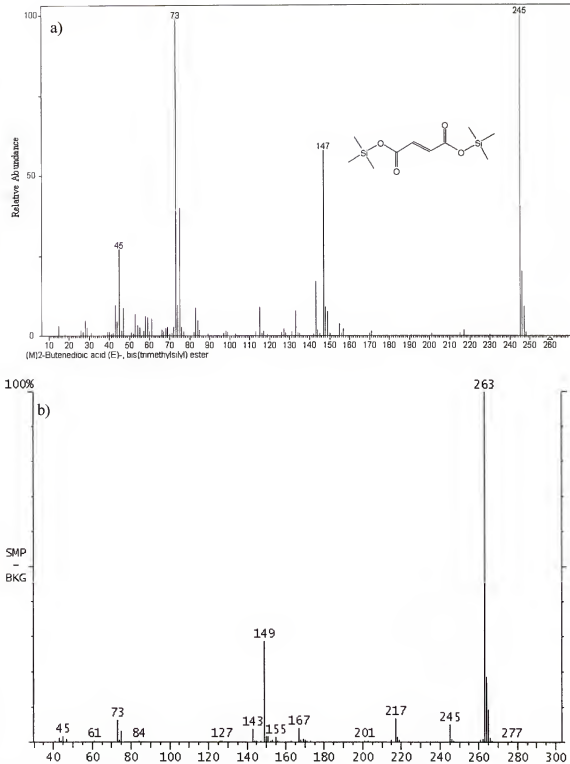

Figure 4-1: Spectra of TMS derivatives of fumaric acid. a) Reference spectrum (NIST#: 78901); b) QITMS spectrum showing missing m/z 147 and additional m/z 149 and m/z 263 due to water reactions.

reference for bis(trimethylsilyl) fumaric acid. The second spectrum of bis(trimethylsilyl) fumaric acid was acquired on the GCQ with typical water vapor in the QIT. Because of the significant differences in peak intensities between spectra acquired on the QITMS and reference spectra, the spectral quality of the QITMS is often called into question. Knowing that these spectral differences can be explained by the water present in the QIT can help in understanding which ions need to be used for quantitation and thus permit reliable quantitative results to be obtained when analyzing compounds which undergo ion/molecule in the ion trap. For example, the m/z 147 ion is commonly used for quantitation in quadrupole spectra. In the QITMS spectra, the sum of m/z 147, and its reaction products with water, m/z 149 and m/z 151, should give similar accuracy, even if the amount of water in the background is changing during an analysis and the relative intensities of these ions are not reproducible.

Figure 4-2 shows another example of ion/molecule reactions involving water in the QITMS. In the GCQ spectrum, most of the methylene chloride molecular ions are lost to protonate water neutrals in the background. Molecular ions at m/z 84 and 86 decrease in intensity while m/z 19 increases. The m/z 19 ion cannot be used for quantitation, however, because the IonRf is typically too high to efficiently keep the m/z 19 ion in the trap during full scan (the lowest IonRf by default is 21). Also, m/z 19 can come from other ion/molecule reactions and is thus not a specific indicator of the amount of methylene chloride molecular ions injected into the QITMS. MS/MS experiments in which the IonRf was lowered to efficiently trap m/z 19 do reveal that the decrease in molecular ion intensity directly corresponds to an equal increase in m/z 19 intensity. The methylene chloride $[M\text{-}Cl]^+$ fragment ions at m/z 49 and m/z 51 do not react as efficiently

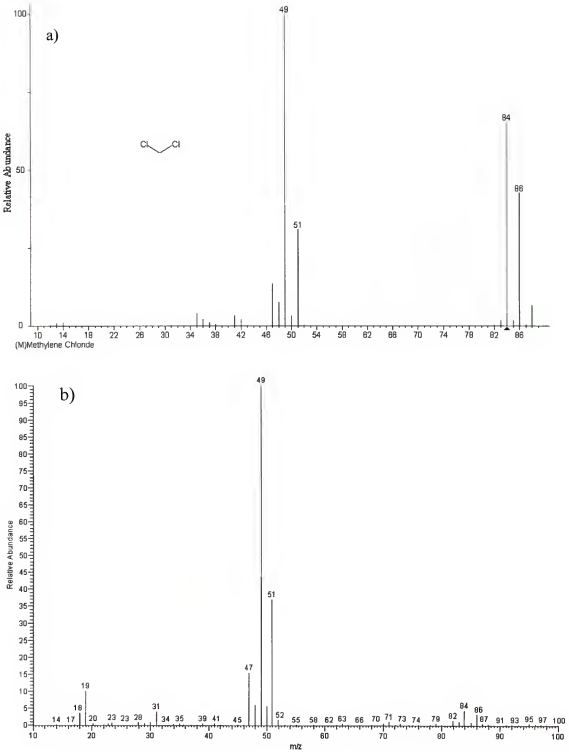

Figure 4-2: Methylene chloride spectra. a) Reference spectrum (NIST#: 61170); b) GCQ spectrum.

with water as the molecular ions. Therefore, in the QITMS, these ions may be monitored for quantitation.

This chapter describes the calibration and use of a residual gas analyzer (RGA) to measure the water in the QITMS. Some common water reactions with ordinary air/water background ions are then presented. The chapter concludes with a description of the TMS acid derivative ion/molecule reactions with water, and their possible use as hygrometers.

Argon and Water Sensitivity on the RGA

A Balzers (Hudson, NH) Prisma QME 200 residual gas analyzer (RGA) was used in all water pressure measurements. The test report for the RGA reported the argon sensitivity to be 8.216×10^{-4} A/Torr at $P_{argon} = 4.5\times10^{-7}$ Torr. Several tests were performed to check the factory sensitivity value and measure the RGA sensitivity for water. Using the Faraday detector with the dwell set to 1 s/amu, the ion current was measured for m/z 20, 40, 17, and 18. A Granville-Phillips series 330 ionization gauge controller was connected to the analog input of the RGA so that ion gauge pressure (on whatever chamber the RGA was mounted) could be measured and stored along with RGA ion currents.

To measure the water content in the GCQ while acquiring GC/MS data, the RGA was attached directly to the spare transfer line flange. To determine the RGA sensitivity and measure the water content of helium, the RGA was attached to its own chamber, an empty Tremetrics 950 mass spectrometer chamber. This was a heated stainless manifold 11.5" in length by 3.75" inner diameter with Viton o-ring seals on all flanges. The RGA

chamber was pumped out with an Edwards EXT250H turbomolecular pump to achieve baseline pressures in the low 10^{-8} Torr range at 40 °C.

A Granville-Phillips series 203 variable leak valve was connected to the RGA chamber and evacuated to an uncorrected ion gauge pressure of 3.2×10^{-8} Torr. Argon was then admitted through the leak valve and the ion currents were measured along with the ionization gauge pressure. The RGA sensitivity for argon was confirmed by comparing the ion current for the sum of argon m/z 40 and m/z 20 ions (Ar^+ and Ar^{2+}) to the background-subtracted and sensitivity-corrected ion gauge pressure for argon leaked into the RGA chamber.

The Granville-Phillips ion gauge manual (pg. 3-57) lists relative gas sensitivities for various gases including argon and water. The tabulated sensitivity for argon (S_{Ar/N_2}) is 1.29 times and for water (S_{H_2O/N_2}) is 1.12 times the sensitivity of nitrogen. Using these values to correct the RGA argon sensitivity (S_{Ar}, 8.216×10^{-4} A) for the ionization efficiency of water, the RGA water sensitivity (S_{H_2O}) should be 7×10^{-4} A/Torr (4-1).

$$S_{H_2O} = S_{Ar} \times S_{H_2O/N2}/S_{Ar/N_2} = (8.216\times10^{-4}\ \text{A/Torr}) \times 1.12/1.29 = 7.07\times10^{-4}\ \text{A/Torr} \qquad (4\text{-}1)$$

Several attempts were made to check the RGA water sensitivity. First, wet argon was made by bubbling argon through water. The wet argon was then admitted into the RGA chamber through the variable leak valve. Ion currents for argon and water were monitored along with the ion gauge pressure. The argon ion current was used to calculate the partial pressure of argon, which was subtracted from the total ion gauge pressure to get the partial pressure of water. This partial pressure was used to calculate the RGA sensitivity for water. In the second experiment, water was sparged with argon for several

days to saturate the water with argon and hopefully displace other gases. A GC syringe was filled with this water and the water was ejected from the syringe. The wet needle was quickly inserted through a septum into the variable leak valve and removed. The vapor from the wet needle injection was then admitted into the RGA chamber through the leak valve. Again, ion currents were compared to ion gauge readings. Both of these methods required subtracting the partial pressure of argon from the ion gauge reading, so the accuracy was questionable and the precision was poor.

The third method used to determine the RGA water sensitivity was based upon the observation that after several minutes of pumping down the empty RGA chamber, water vapor was the only appreciable species in the RGA spectra. The water ion current was measured as the chamber pumped out from a full vent. Ion currents for other background gases besides water vapor monitored with the RGA dropped to less than 10% of the water ion current within the first few minutes of pumping. After this initial pressure decrease, the primary change in pressure was due to surface desorption and removal of water. A plot of water total ion current versus ion gauge pressure over many hours of pumping gave a slope equal to the RGA sensitivity for water. Figure 4-3 shows a plot of this data.

This method appeared to be the most accurate and agree well with the theoretical sensitivity calculated from the relative ion gauge sensitivities. The sensitivity is 6.5×10^{-4} A/Torr, which is quite close to the theoretical 7×10^{-4} A/Torr. The water ion current used for this plot and all other water measurements represents the sum of ion currents for m/z 17 and 18 (OH^+ and H_2O^+). The x-intercept in this plot represents the background pressure of the other gases present in the RGA chamber.

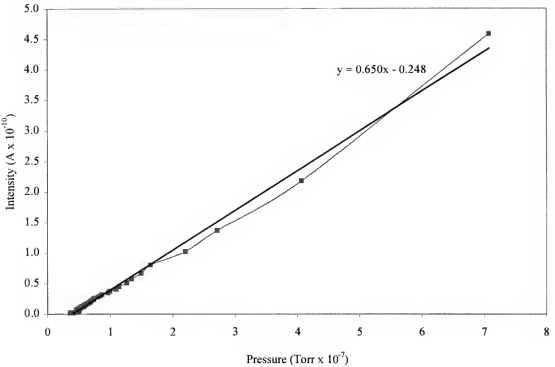

Figure 4-3: Water ion current on the RGA versus corrected ion gauge pressure.

Water in the QITMS from Trapping Helium

The helium conductance for the GCQ ion trap is 3.736 L/s, calculated by Jae Schwartz at Finnigan. Using a helium-to-water-vapor conductance correction factor of 0.478 (H_2O to N_2 1.263 ÷ He to N_2 2.64, Leybold-Heraeus, 1985), this converts to a conductance of 1.787 l/s for water vapor. The pumping speed of the turbomolecular pump is approximately 180 L/s (Chapter 2). If the conductance of the trap is only 1.787 L/s for water vapor, the water partial pressure due to trapping helium will be 100 times (180/1.787) greater inside the ion trap than the water partial pressure in the chamber due to trapping helium. The water pressure in the QIT is only about ten times higher than the total background water pressure in the chamber, however. The partial pressure of water

in the chamber background comes from other sources besides just the trapping helium, such as outgassing of o-rings, and water admitted through the GC column.

In one measurement, the background water pressure in the GCQ chamber was measured to be 1.4×10^{-7} Torr. The background water vapor from introduction with the trapping helium was 1.5×10^{-8} Torr (measured in the separate RGA chamber). The water vapor pressure in the ion trap was therefore 1.6×10^{-6} Torr (4-2), approximately 10 times the background water pressure.

$$((180 \text{ L/s} / 1.787 \text{ L/s}) \times 1.5\times10^{-8} \text{ Torr}) + (1.4\times10^{-7} - 1.5\times10^{-8}) \text{ Torr} = 1.6\times10^{-6} \text{ Torr} \quad (4\text{-}2)$$

Air/Water Spectra

Most of the m/z 19 ions seen in air/water spectra on the GCQ are produced in the ion trap through ion/molecule reactions, as discussed below. They can also come from the ion source under high-pressure conditions such as CI. Nitrogen is one major contributor to the production of m/z 19 through the following reactions (Harrison, 1983, p.64).

$$N_2^{+\cdot} + 2\,N_2 \rightarrow N_4^{+\cdot} + N_2 \quad (4\text{-}3)$$

$$N_4^{+\cdot} + H_2O \rightarrow H_2O^{+} + 2\,N_2 \quad (4\text{-}4)$$

$$H_2O^{+} + H_2O \rightarrow H_3O^{+} + OH^{\cdot} \quad (4\text{-}5)$$

Table 4-1 shows the results of an MS/MS experiment to see what ions in air/water produce m/z 19. Each ion was isolated and allowed to react for the normal CID period of 15 ms with no CID resonant excitation. The product ions were then scanned from m/z 10 to 60. The ion at m/z 29, which is also a very efficient reagent for m/z 19 production, is

most likely $C_2H_5^+$, which appears to be a fragment ion from source contaminants introduced via the GC.

Table 4-1: Reactions of isolated air/water ions to determine which ions form m/z 19. Base peak and intensities represent product spectra.

Isolated m/z	Base peak	Base Intensity	m/z 19 Intensity	m/z 19 % Relative Int.
14	28	41	0	0
15	28	76	0	0
17	18	42	0	0
18	18	100	23	23
19	28	80	16	20
28	28	38000	17100	45
29	19	27000	27000	100
30	30	6100	305	5
32	32	300000	2100	1
33	19	730	730	100
40	40	10000	2700	27
41	41	2700	378	14
44	44	7400	2368	32
45	45	2700	1944	72
51	51	330	99	30
55	55	1100	77	7
56	56	280	90	32
57	57	510	92	18

In the GCQ air/water spectra, m/z 19 intensities show a linear response to background water partial pressure in the chamber measured with the RGA, as seen in Figure 4-4. If the amount of air and water present in the ion trap from the trapping helium were to remain constant from one helium tank to the next, the m/z 19 intensity could be calibrated to background water pressure and used to gauge the water present in the background. The problem with this is that many ions (as shown in Table 4-1) produce m/z 19. Without performing this calibration each time the helium is changed, it is difficult to measure the amount of water actually present in the chamber because the

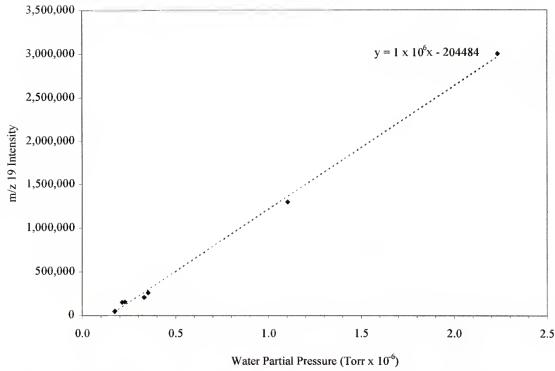

Figure 4-4: Intensity of air/water m/z 19 ions versus water pressure in the GCQ chamber. The x-intercept may be the partial pressure of water in the chamber at which too few ion/molecule collisions with water occur in the reaction time to form m/z 19 in the trap.

m/z 19 intensity is very susceptible to changes in injection parameters and concentrations of other background ions.

The following spectra are presented to show that helium admitted into the GCQ often contains air and water. Because the helium admitted into the QIT often contains air and water, the spectra make it appear that there is a leak in the vacuum system. These spectra also reveal the differences between quadrupole RGA spectra and QITMS spectra for air and water.

The spectrum in Figure 4-5 was acquired on the RGA by leaking atmospheric air through the restrictor capillary into the RGA chamber. This shows what an air leak looks

like on a quadrupole for comparison with QITMS (which will be shown below). The lab's air handling system reported 44% relative humidity and 24 °C when the air-leak spectrum was acquired. At this temperature, the saturation vapor pressure of water is 22.3 Torr (Leybold-Hereaeus, 1985, p.94). At this humidity, the partial pressure of water in atmosphere is therefore 9.8 Torr (0.44 × 22.3 Torr). This means the sum of ions due to water (H_2O^+, OH^+, and O^+) should equal about 1.6 % (P_{H2O}/P_{N2} = 9.8 Torr/ 594 Torr = .016) of the sum of ions due to nitrogen (N_2^+, $^{14}N^{15}N^+$, N^+, and N_2^{++}).

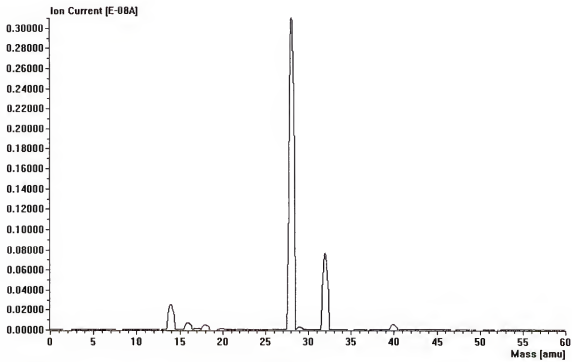

Figure 4-5: Air spectrum acquired with the RGA.

The top spectrum in Figure 4-6 shows the background acquired with the RGA mounted on a turbo pumped GCQ. The GCQ has air flowing into the instrument with the helium, causing the air peaks to be observed. This is not due to a leak. The bottom spectrum in Figure 4-6 is a background subtracted spectrum of helium acquired with the

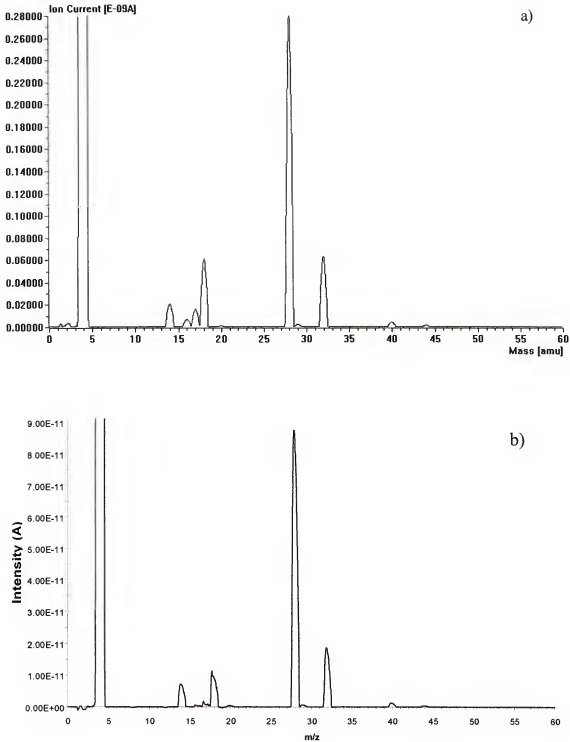

Figure 4-6: Spectra of helium background acquired with the RGA. a) RGA spectrum of GCQ background; b) Background-subtracted spectrum of helium in the RGA chamber.

RGA on the separate RGA chamber showing the air and water content of the helium. To obtain this background subtracted spectrum, a reference spectrum was acquired with the helium pressure set to 0 psi on the capillary restrictor flowing helium into the RGA chamber. The reference spectrum was then subtracted from another spectrum taken with 5 psi helium on the capillary restrictor.

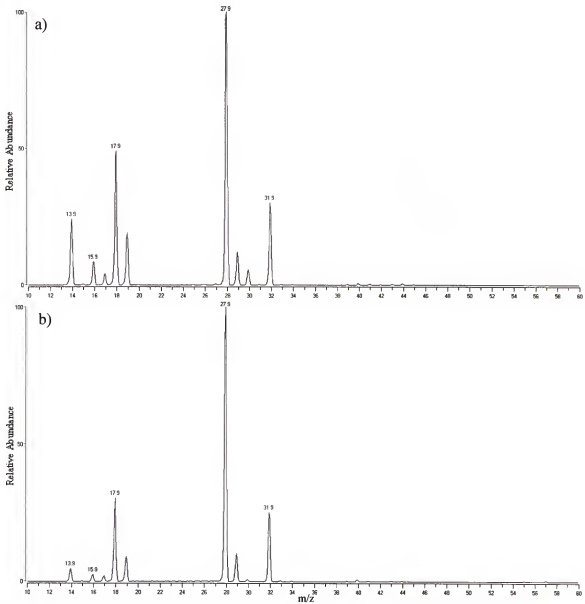

Figure 4-7: Air/water spectra acquired on a relatively dry GCQ. a) With a turbomolecular pump; b) With a diffusion pump.

The GCQ QITMS spectra of air/water ions acquired on an instrument with a turbo pump and diffusion pump shown in Figure 4-7 are presented for comparison with the RGA spectra as in Figure 4-6 a). The nitrogen peak at m/z 28 decreases on the QITMS as m/z 18 and 19 from water increase. It was noted that the spectra in Figure 4-7 were obtained on a relatively dry GCQ. This is relative to typical water vapor levels such as in the instrument used to acquire the air/water spectrum in Figure 4-8.

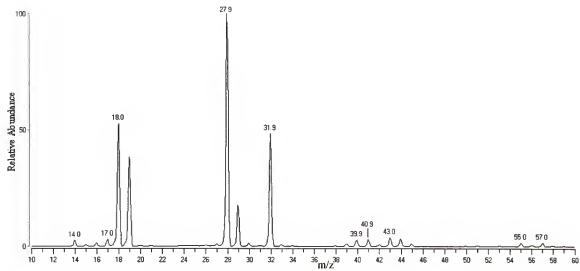

Figure 4-8: Air/water spectrum acquired on the GCQ with normal water vapor in the QITMS.

Typically, a GCQ air/water spectrum will have m/z 19 at least as intense as m/z 18. Extra peaks, such as m/z 29, 30, 41,... etc., also appear in the QITMS spectra from hydrocarbon background in the source. The decrease in m/z 28 with the increase in m/z 19 is much more dramatic when the water is more concentrated in the ion trap such as in Figure 4-8. Still, the relative intensities observed for air ions (such as m/z 28) that react with water are highly dependent upon their concentration in the trapping helium and not

just the water pressure. Making spectral comparisons (with relative intensities of air/water ions) between different GCQ instruments is almost futile.

Trimethylsilyl Derivatives of Organic Acids

Experimental

The succinic acid, fumaric acid and derivatizing reagents were purchased from Supelco as part of an organic acids standard kit. The acids were derivatized by the following procedure:

- A stock solution was prepared from 64 mg fumaric acid ((E)–butenedioic acid, molecular weight 116) and 53 mg succinic acid (butanedioic acid, molecular weight 118), weighed out and dissolved in 50 ml ethyl alcohol (bp 78.5 °C).
- A 100 μL aliquot of the 1 mg/mL stock solution was placed into a screw-capped vial and evaporated to dryness under argon.
- Aliquots, 50 μL each, of bis(trimethylsilyl) trifluoroacetamide (BSTFA) and pyridine were mixed with the acid residue and heated to 50 °C for at least an hour in the GC oven.

For GC analysis, 10 μL of the derivatized acid solution were diluted with 1 mL hexane. Injections of 1 μL were injected in split mode into the GC. Most of these data were acquired with the split set to 15 mL/min and the carrier gas set to constant flow (1mL/min). The injector was set to 250 °C, the transfer line was set to 275 °C, and the ion source was set to 175 °C. The GC temperature program consisted of an initial ramp from 50 °C to 275 °C at 10 °C/min and a hold for 10 min at 275 °C.

TMS Derivative Spectra

Figure 4-9 shows the NIST reference spectra for the TMS derivatives. The m/z 147 ion was chosen for the water reaction studies, because it is often replaced by m/z 149 in the QITMS (as in Figure 4-1). Figures 4-10 and 4-11 show the differences observed in the QITMS spectra of the TMS derivatives between wet and dry instruments. The wetness of the instruments is used as a qualitative description. It is based upon several factors, the actual partial pressure of water in the instrument, the amount of m/z 19 in the air/water spectra, and the extent of the ion/molecule reaction with the TMS derivatives. Using the TMS m/z 149/147 intensity ratio in full scan mode to define wetness, the instrument typically falls into the wet category when the intensity of m/z 147 ion is less than the intensity of the m/z 149 ion. Likewise, the instrument is relatively dry when the m/z 147 ion is more abundant than the m/z 149 ion. It must be pointed out that water was never intentionally added to the GCQ to obtain wet spectra. All efforts were made to keep the water vapor to a minimum. Wet spectra were often acquired as the instrument was pumping down from a vent to atmosphere. At least 25 hours were typically required to pump a normally dry instrument down after venting to obtain spectra that would put the instrument in the dry classification.

The m/z 147 ion is formed by the rearrangement for bis(trimethylsilyl) succinic acid, as proposed in Figure 4-12 (McLafferty, 1980). The m/z 147 fragment ion readily exchanges an -OH for a $-CH_3$ group when it contacts water in the ion trap, forming the m/z 149 ion. The m/z 149 ion can then exchange another -OH for a $-CH_3$, forming m/z

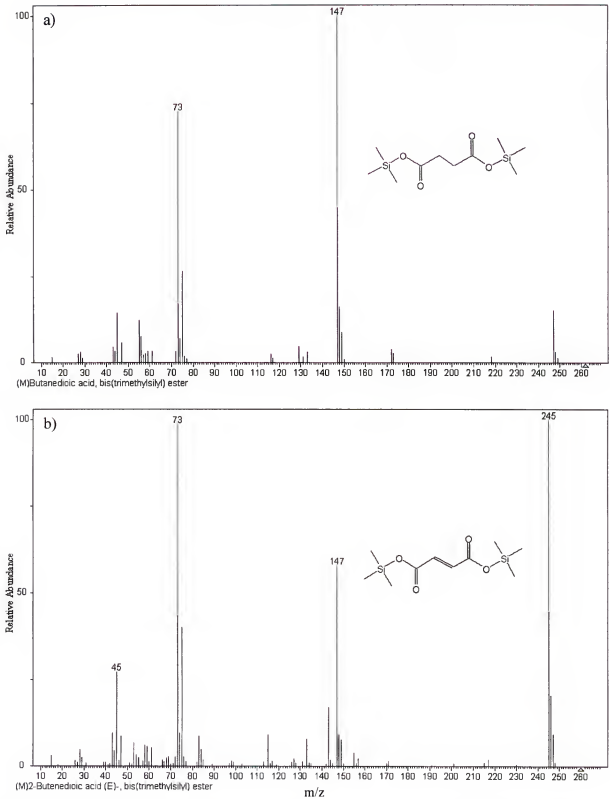

Figure 4-9: Reference spectra for the TMS derivatives. a) Succinic acid (NIST#: 30796); b) Fumaric acid (NIST#: 78901).

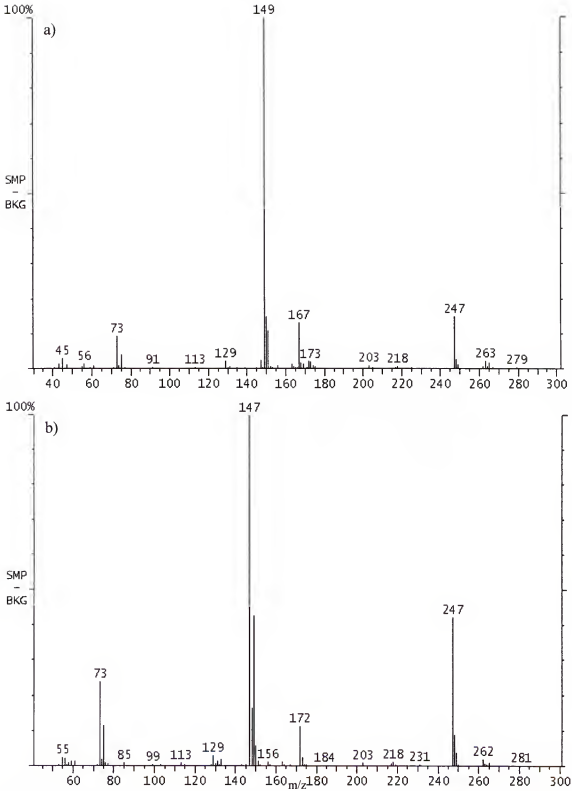

Figure 4-10: Spectra of TMS derivative of succinic acid on the GCQ QITMS. a) Spectrum acquired with high water vapor; b) Spectrum acquired with low water vapor.

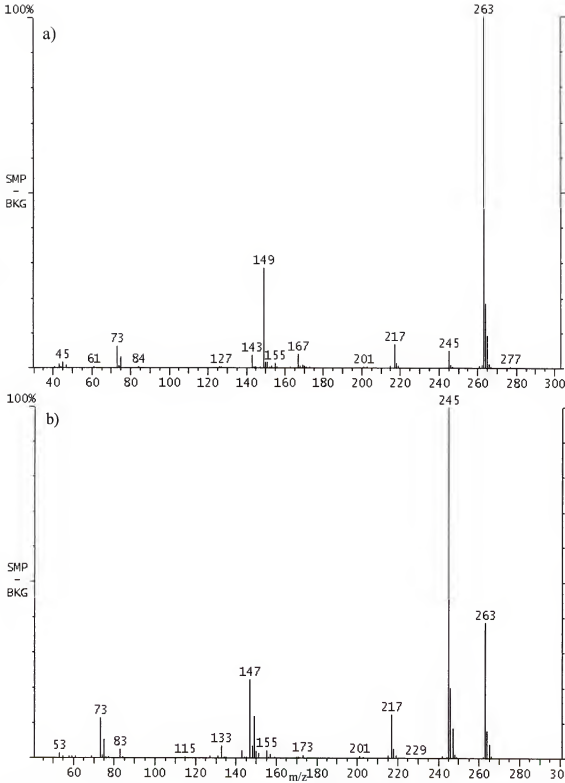

Figure 4-11: Spectra of TMS derivative of fumaric acid on the GCQ QITMS. a) Spectrum acquired with high water vapor; b) Spectrum acquired with low water vapor.

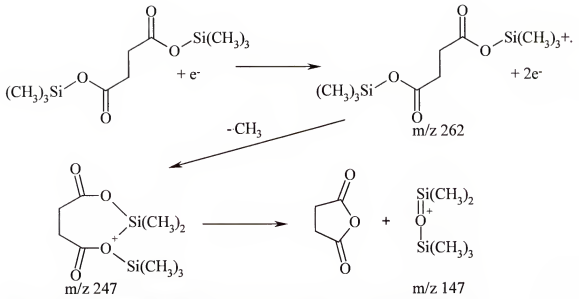

Figure 4-12: Proposed structures for bis(trimethylsilyl) succinic acid ions.

151. An ion can even be observed at m/z 153 if the water concentration is high, or if sufficient time is allowed for another reaction.

An ion appears at m/z 263 in the fumaric acid derivative spectra becoming the base peak when enough water is present. Some m/z 263 ions also appear in the spectra of the succinic acid derivative when the sample concentration is high. Split injections of 1 μg and 10 ng were studied to see if there was a difference in the formation of either acid's m/z 263 ion in the ion source due to concentration differences. The 1 μg injection showed much higher relative intensity for m/z 263 than did the 10 ng injection for the succinic derivative, but there was no change in m/z 263 for the fumaric acid derivative. The AGC target in the QITMS was equal for both injections. This strongly suggests that the m/z 263 was formed in the ion source, since the number of ion injected into the trap was constant regardless of the source concentration (because automatic gain control was used). For the fumaric derivative (MW 260) the 263 ion is most likely a water adduct

with m/z 245, the $[M- 15]^+$ ion. The water adduct of the $[M- 15]^+$ ion (m/z 247) of the succinic derivative (MW 262) would fall at m/z 265 instead of m/z 263. Because there is not an intense ion at 265, and the amount injected only affects the formation of m/z 263 for the succinic derivative, the two derivatives probably undergo different reactions to form m/z 263. The formation of m/z 263 for the succinic derivative appears to be protonation to form the [M+H]+ ion occurring in the source, while for the fumaric derivative m/z 263 appears to result from an ion/molecule reaction with water in the trap. MS/MS of m/z 263 showed loss of H_2O to form a fragment ion at m/z 245 for the fumaric derivative only. The succinic derivative (m/z 263) ion formed an intense fragment at m/z 173, due to loss of $(CH_3)_3SiOH$, consistent with m/z 263 being the [M+H]+ ion.

Use as a Hygrometer

The spectra of the TMS derivatives in the QITMS qualitatively reveal the water content in the ratio of their m/z 147 and m/z 149 ions. The following section describes experiments used to investigate the relationship between the TMS/water reactions and the partial pressure of water and to determine the reaction order.

As mentioned above, the m/z 147 ion is lost as it reacts with water to form m/z 149 and m/z 149 is lost as it reacts with water to form m/z 151. Figure 4-13 shows data collected for these ion/molecule reactions for the TMS derivative of succinic acid at two ion concentrations in the trap (AGC targets of 50 and 1), and two different reaction IonRf levels. Unless labeled as full scan, the data represent MS/MS reactions of the isolated ions at m/z 147. Relative intensities represent the mass chromatographic peak area of the individual ion (m/z 147, 149, or 151) divided by the sum of mass areas for m/z 147, 149,

and 151. The full scan data deviate from the MS/MS AGC 50 data. This difference may be explained by competing side reactions with water since the other ions have not been removed from the trap. Also, the exact reaction time is indeterminant in the full scan data because there is no isolation step, and thus ions can react from the time they are formed in the source until they are ejected from the trap. The data for the ions at AGC targets of 1 are also not perfectly linear. This is because AGC had difficulty adjusting the ionization time for this concentration. The ionization time required to meet the target concentration was just below the minimum range of the adjustable ionization time; therefore, the ionization time was fixed at a constant minimum level (0.029 ms), and a few more ions were injected into the QIT for some data points. These data could be reacquired with less sample injected into the ion source to obtain better linearity.

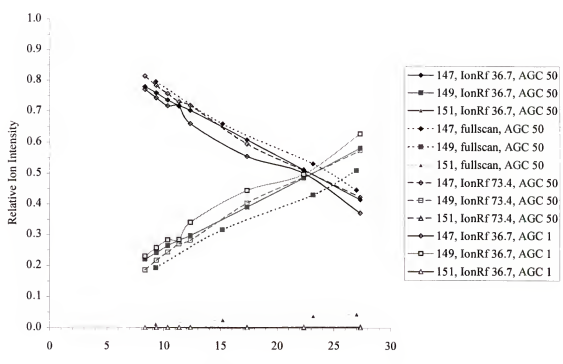

Figure 4-13: Succinic acid TMS derivative m/z 147, 149, and 151 ions versus reaction time.

The data for figure 4-13 were taken with a new molecular sieve trap on the trapping helium, so the water concentration was lower than in a standard instrument. It was still easy to observe the reactions with water. This chart shows that the m/z 147 intensity can be dramatically increased by lowering the reaction time in the ion trap, and that the ion ratios do not change considerably with ion concentration (this is indicative of a first order reaction, the rate is directly proportional to concentration).

The plot below (Figure 4-14) presents similar MS/MS data as shown in Figure 4-13, with the ratio of m/z 149 to m/z 147 plotted versus reaction time. As shown on the left axis, the reference spectra have 149/147 ratios of 0.090 for bistrimethyl succinic acid, and 0.135 for bistrimethyl fumaric acid. The isotopic ratios relative to m/z 147 for these

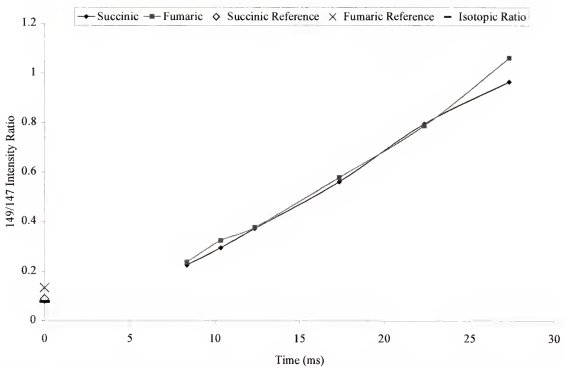

Figure 4-14: Intensity ratios for m/z 149/147 ions of TMS derivatives versus reaction time.

two ions (given the natural abundances ^{13}C, ^{2}H, ^{17}O, ^{18}O, ^{29}Si, ^{30}Si) should be 0.079 for m/z 149, and 0.0016 for m/z 151. Therefore, the NIST reference spectra have m/z 149/147 ratios higher than the isotopic ratio. This suggests that some reaction with water could be occurring in the reference instrument as well.

By changing the AGC target, the number of ions within the ion trap changes. Figure 4-13 demonstrates no significant change in ion ratios due to change in ion concentration. All but the full scan data for m/z 147 and 149 meet at the same point (m/z 149/147 ratio ~ 1) in Figure 4-13. This suggests that the reaction is first order with respect to ion concentration. As the ion concentration is doubled, the reaction rate is doubled, keeping the same ratio of products to reactants. Running an analysis at several AGC targets and constructing a van't Hoff plot proved this hypothesis. The natural log of the rate (# of 147 ions trapped - # of 147 ions after reaction time / reaction time) was plotted versus the natural log of the number of m/z 147 ions. The slope of a van't Hoff plot gives the order of reaction with respect to the species whose concentration is plotted. The van't Hoff plot in Figure 4-15 shows the reaction to be first-order with respect to initial number of m/z 147 ions from both succinic acid and fumaric acid.

A van't Hoff plot (Figure 4-16) was also constructed to evaluate whether the reaction was first-order with respect to water concentration as well. To get the water concentration for this plot, the background water pressure was measured as the samples were analyzed. The partial pressure of water in the ion trap was assumed to be the sum of the background partial pressure and a constant pressure due to the flow of wet helium into the trap estimated from RGA helium data. The AGC target was held constant so that the

rate change reflected the change due to decreasing water concentration as the instrument pumped down.

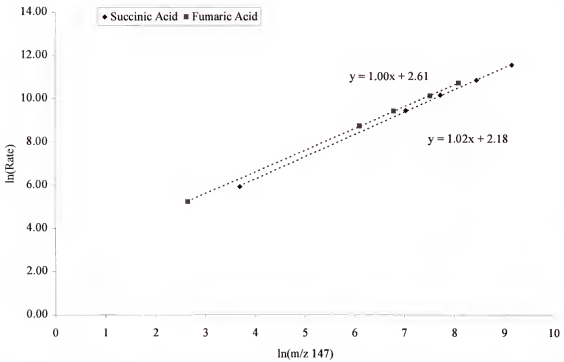

Figure 4-15: Van't Hoff plot for determining the order of the ion/molecule reaction between m/z 147 ions and water with respect to the ion density. The lines and equations are from the linear regression.

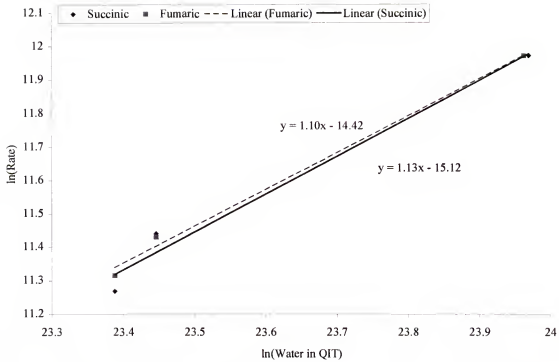

Figure 4-16: Van't Hoff plot for determining the order of the ion/molecule reaction between m/z 147 ions and water with respect to the water concentration. The lines and equations are from the linear regression.

This plot was used here to determine the reaction order, but it could also be used to determine the water concentration as well. (Ideally, this experiment should be repeated and more data points should be included in the plot.) Once the rate is determined from the TMS spectra, the pressure of water in the trap can be calculated from the equations in the figure. The rate is equivalent to the number of 147 ions lost within the trap divided by the reaction time. The water concentration above equals the number (n) of water molecules in the center of the ion trap (V), where the ions should be contained. It was approximated from the ideal gas law (n=PV/RT) using the partial pressure (P) of water from RGA calculations and a volume of 0.25 ml and a temperature of 298 K.

The plot in Figure 4-17 shows the effect of increasing the helium flow via pressure on the restrictor. As expected, the increased helium flow increased the water concentration in the trap; the reaction with m/z 147 caused the m/z 149 intensity to increase. This confirms other measurements that show the helium contains water vapor. Other experiments not presented in this dissertation revealed that the best strategy to reduce water vapor in the QIT was to eliminate the water from the trapping helium. This is consistent with the conductance argument presented earlier.

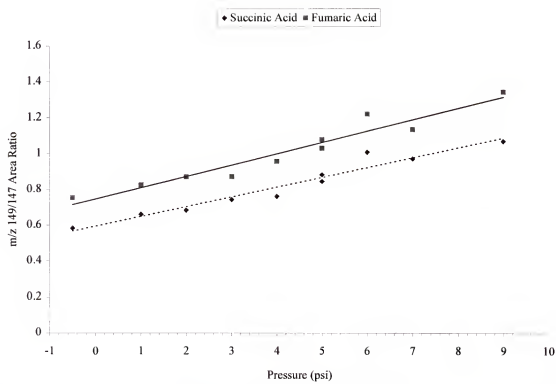

Figure 4-17: Plot of m/z 149/147 peak area ratios for TMS derivatives versus head pressure on the helium restrictor.

Conclusions

The mass spectra of the TMS acid derivatives offer conclusive evidence that ion/molecule reactions with water occur in the QITMS, and that these reactions can be qualitatively and quantitatively correlated with selective reactions within the QIT. Furthermore, ion/molecule reactions change the appearance of spectra obtained with the QITMS by varying the relative abundance of and/or adding new fragment and product ions. They pose a problem in spectral reproducibility from instrument to instrument that can only be overcome by appropriate knowledge of the reactions and their products. By making use of the spectral hygrometers mentioned here, the amount of water in the QITMS can be approximated prior to analysis of other compounds and the amount of water reactions that will be encountered can be predicted.

Careful examination of the above ion/molecule reactions reveals the importance of AGC for maintaining good spectral reproducibility during analysis of compounds in a QITMS with a stable water vapor pressure. If AGC were not used, the concentration of ions injected into the QITMS would vary across chromatographic peaks, causing huge shifts in the relative abundance of reactive ions. The linearity in data from single injections plotted in Figure 4-15, where the concentration of ions in the trap was calculated from the AGC target concentration and the full scan ion currents, reveals just how well AGC can regulate ion concentration in the QITMS.

The m/z 147 fragment ion from fumaric acid appears to be more reactive than the same fragment ion from succinic acid. This is suggested by the higher m/z 149/147 ratio in the data above, including the NIST reference data. There may be several explanations

for the difference in reactivity. One could simply be that the fumaric derivative is maintained on the GC column longer than the succinic derivative so it may be introduced at a higher temperature; however, all molecules pass through the transfer line at the same temperature before entering the source, so this may not be significant. Another plausible explanation is that the m/z 147 fragment ions have different internal energies because they are formed from different parent ions. Either explanation suggests that the ions retain internal energy differences over a long time in the QITMS. This is promising for future studies of ion/molecule reactions designed to separate isomers formed by different processes.

CHAPTER 5
CONCLUSIONS AND FUTURE WORK

This dissertation described two QITMS instruments with ion injection and demonstrated the utility of these instruments for the study of ion/molecule reactions. These reactions were able to reveal some of the advantages of using ion injection with the QITMS. Neutral background was kept to a minimum inside the ion trap, reducing competitive reactions. The spatial separation of the ion source from the ion trap allowed study of reactions involving CI produced ions, which may not have been possible with internal ionization in the QITMS. The high pressure required for CI production of some reagent ions in the source did not require an increase in the ion trap pressure. The number of reagent ions for ion/molecule reactions was precisely controlled not by the amount of neutral injected into the source, but by a well-controlled injection time into the trap (AGC). Precise control of the reagent ion concentration made possible the measurement of reaction kinetics, as in the case of the ion/molecule reactions with water, which clearly show time- and concentration-dependence. In addition to the advantages offered by ion injection were the benefits already offered by using an ion trap for investigating ion/molecule reactions. These benefits, including the ability to trap and hold select numbers of ions at specific m/z for long periods of time in the presence of reacting neutrals, and the ability to select specific reactions times, made the QITMS well suited for this work.

The ion injection instrumentation was shown to allow the study of gas-phase ion-neutral chemistry between chiral reagent ions and chiral neutrals. Enantioselectivity, however, was not definitively observed for the chiral ion/molecule reactions. Winkler et al. (1994) observed chiral selectivity in the homochiral and heterochiral protonated dimers of dimethyl tartrate. In these species the difference in their calculated association energies was 0.22 kcal/mol. This was attributed to an additional hydrogen bond between the homochiral tartrates. This energy difference is on the same order as the energy differences calculated for the chiral Diels-Alder products in Chapter 3. It may be possible that a difference this low in adduct stability may not be observable in the QITMS due to greater stabilizing or fragmenting effects of collisions with the helium buffer gas on weakly-bound complexes. First-order ion/molecule reactions between TMS derivatives and water presented in Chapter 4 did, however, suggest that some internal energy differences are retained after ionization long enough to observe in the QITMS. The reaction rates of the m/z 147 ion from the succinic acid derivative and fumaric acid derivative were not the same.

The selective ion/molecule reactions with isopinocampheol and phenylethylamine studied in the SweetP ion injection instrument were not enantioselective as observed in the ion trap full scan spectra. MS/MS of the reaction products produced within the ion trap did not exclude the possibility of enantioselectivity in the CI product ion fragmentation pathways. In fact, similar fragmentation trends were observed for MS/MS of m/z 258 ions reported by Sellier et al. (1994).

The possibilities for future ion/molecule reaction studies on the SweetP and GCQ instruments are numerous. For future investigations related to the work in this

dissertation, the following suggestions are made. The use of MALDI or LDCI for ionization of the acetonides may be attempted to more efficiently get these species into the ion trap as ions. Also, the SweetP instrument could be modified to allow introduction of neutrals into the ion trap through a GC, which may offer added stability by controlling the amount of neutral introduced into the QIT, and possibly allow rapid switching between enantiomers separated on a chiral GC column. The trap conductance would have to be changed to accommodate the higher carrier gas load.

The acetonides with HOMO-LUMO energy gaps closer to the other Diels-Alder reaction products mentioned in Chapter 2 may be investigated to determine if the somewhat greater energy gaps produce less fragmentation upon reaction. If less fragmentation of the Diels-Alder ion/molecule product is observed, the intact reaction products may be further studied for enantioselectivity.

The ion injection instruments may, of course, be used to study other compounds known to show enantioselectivity in the gas phase to determine if steric hinderance and small thermodynamic differences in adduct stability can be observeded in the QITMS. Different ionization methods may be incorporated into the SweetP instrument such as fast atom bombardment (FAB) mass spectrometry and electrospray ionization (ESI). Attempts may be made to duplicate reactions that are reported to show enantioselective recognition using these ionization techniques. For example, chiral crown ethers studied by Sawada et al.(1993) and Pocsfalvi et al. (1996) were reported to demonstrate selective host-guest complexation with enantiomeric primary ammonium cations in FAB mass spectrometry. Dearden et al. (1997) were able to demonstrate host-guest chiral

discrimination between enantiomeric amines and dimethyldiketopyridino-18-crown-6 ionized by ESI in a Fourier transform ion cyclotron resonance mass spectrometer.

Protonated trimers of enantiomeric amino acids formed by FAB were studied by MS/MS and found to form different ratios of protonated dimers (Vekey and Czira, 1997). This chiral discrimination was related to the gas-phase basicities of the homochiral and heterochiral dimers. The same trimers and dimers may be able to be formed and studied from ions and neutrals injected into the QITMS.

Compounds used for chromatographic separation of enantiomers in liquid chromatography and gas chromatography may be able to be used for ion/molecule reactions in the QITMS. Dobashi et al. (1991) have reported a number of enantiomeric compounds that are resolved by capillary gas chromatography on a chiral stationary phase consisting of (R,R) tartramide bound to a polysiloxane backbone. Separation is reported to occur by differences in hydrogen bonding and steric hinderance. In this work, 1,2 diols were reported to demonstrate good separation on the chiral stationary phase. The incorporation of these interactions into a gas-phase reaction may be of interest in the QITMS instruments described in this dissertation to separate enantiomeric ions. The same functional groups and reactions may be able to be studied with derivatization of these species to increase volatility.

Other future work may explore the spectral differences that are known to exist between many instruments for fragments ions produced by CI. Ong and Hites (1992) suggest that electron capture negative ion mass spectra are not reproducible from one instrument to another (even when populations of thermal electrons are similar) because of differences in extraction efficiencies of ions from different sources. This is plausible;

however, there may be other considerations such as water pressure in the ion source. Selective ion/molecule reactions with water should be explored to determine the effects of water content in the ion source on spectral quality and reproducibility of CI produced ions which are known to have irreproducible fragment ion ratios.

GLOSSARY

AC	Alternating current.
AGC	Automatic gain control.
CI	Chemical ionization.
CID	Collision-induced dissociation.
DAC	Digital-to-analog converter.
DC	Direct current.
EHT	Extended-Hückel theory.
EI	Electron ionization.
ESI	Electrospray ionization.
FAB	Fast atom bombardment.
FC43	Fluorocarbon 43, perfluorotributylamine.
GC	Gas chromatograph(y).
GCQ	Finnigan quadrupole ion trap mass spectrometer with ion injection.
HOMO	Highest occupied molecular orbital.
IonRf	Radiofrequency amplitude (lowest mass-to-charge stable in the trap).
ITS40	Finnigan quadrupole ion trap mass spectrometer.
LDCI	Laser desorption chemical ionization.
LUMO	Lowest unoccupied molecular orbital.
m/z	Mass-to-charge ratio.

MALDI	Matrix-assisted laser desorption ionization.
MM+	Molecular mechanics plus.
MS	Mass spectrometry.
MS/MS	Tandem mass spectrometry.
MS^n	Tandem mass spectrometry to the nth power.
MW	Molecular weight.
NCI	Negative chemical ionization.
NIST	National Institute of Standards and Technology.
PCI	Positive chemical ionization.
QIT	Quadrupole ion trap.
QITMS	Quadrupole ion trap mass spectrometer.
RF	Radiofrequency.
RGA	Residual gas analyzer.
S/N	Signal-to-noise ratio.
SIM	Selected ion monitoring.
TIC	Total ion current.
TMS	Trimethylsilyl.
TSQ	Finnigan triple quadrupole mass spectrometer.
TTL	Transistor-transistor logic.
V_{O-P}	Zero-to-peak voltage.
V_{P-P}	Peak-to-peak voltage.

LIST OF REFERENCES

Basic, C.; Eyler, J.R.; Yost, R.A. *Org. Mass Spectrom.*, **1994**, 29, 329.

Berberich, D.W. Ph.D. Dissertation, University of Florida, Gainesville, FL, **1989**.

Brodbelt, J.S. Chapter 5: Effects of Collisional Cooling on Ion Detection, In March, R.E.; Todd, J.F.J. (Eds.) *Practical Aspects of Ion Trap Mass Spectrometry*, Vol. I, CRC Press, Boca Raton, FL, **1995**, pp. 375-399.

Chapman, J.R. *Practical Organic Mass Spectrometry*, 2nd Ed., John Wiley & Sons, New York, **1994**.

Coopersmith, B.I. Ph.D. Dissertation, University of Florida, Gainesville, FL, **1994**.

Dawson, P.H.; Whetten, N.R. *Int. J. Mass Spec. Ion Phys. 2*, **1969**, 45.

Dearden, D.V.; Dejsupa, C.; Liang, Y.; Bradshaw, J.S.; Izatt, R.M. *J. Am. Chem. Soc.*, **1997**, 119, 353.

Denekamp, C.; Weisz, A.; Mandelbaum, A. *J. Mass Spectrom.*, **1996**, 31, 1028.

Depuy, C.H.; Gronert, S.; Mullin, A.; Bierbaum, V.M. *J. Am. Chem. Soc.*, **1990**, 112, 8650.

Dobashi, Y.; Nakamura, K.; Saeki, T.; Matsuo, M.; Hara, S.; Dobashi A. J. Org. Chem. **1991**, 56, 3299.

Eberlin, M.N.; Cooks, R.G. *J. Am. Chem. Soc.*, **1993**, 115, 9226.

Fales, H.M.; Wright, G.W. *J. Am. Chem. Soc.*, **1977**, 99, 2339.

Griffin, T.P. Ph.D. Dissertation, University of Florida, Gainesville, FL, **1995**.

Harrison, A.G. *Chemical Ionization Mass Spectrometry*, 2nd Ed., CRC Press, Boca Raton, FL, **1992**.

Honovich, J.P.; Karachevtsev, G.V.; Nikolaev, E.N. *Rapid Commun. Mass Spectrom.*, **1992**, 6, 429.

Hudlicky, T.; Boros, C.H. *Tetrahedron Lett.*, **1993**, Vol. 34, 16, 2557.

Johnson, J.V.; Basic, C.; Pedder, R.E.; Kleintop, B.L.; Yost, R.A. *Chapter 8: Energetics and Collision-Induced Dissociation Efficiencies in the Quadrupole Ion Trap Mass Spectrometer,* In March, R.E.; Todd, J.F.J. (Eds.) *Practical Aspects of Ion Trap Mass Spectrometry*, Vol. lll, CRC Press, Boca Raton, FL, **1995**, pp. 257-312.

Johnson, J.V.; Yost, R.A.; Kelly, P.E.; Bradford, D.C. *Anal. Chem.*, **1990**, 62, 2162.

Leybold-Heraeus Catalogue HV 250, "Vacuum Technology: Its Foundations, Formulae and Tables," San Jose, CA, 1985.

Lu, L.; Yang, S.S.; Wang., Z.; Cooks, R.G.; Eberlin, M.N. *J. Mass Spectrom.*, **1995**, 30, 581.

March R.E.; Hughes, R.J. *Quadrupole Storage Mass Spectrometry*, John Wiley and Sons, New York, **1989**.

March, R.E.; Londry, F.A. Chapter 2: Theory of Quadrupole Mass Spectrometry, In March, R.E.; Todd, J.F.J. (Eds.) *Practical Aspects of Ion Trap Mass Spectrometry*, Vol. l, CRC Press, Boca Raton, FL, **1995**, pp. 28-41.

McLafferty, F.W. *Interpretation of Mass Spectra*, 3rd ed., University Science Books, Mill Valley, CA, **1980**, pp. 171-172.

Moore, R.B.; Gulick, S. *Physica Scripta*, **1988**, T22, 28.

Nikolaev, E.N.; Goginashvili, G.T.; Tal'rose, V.L.; Kostyanovsky, R.G. *Int. J. Mass Spectrom. Ion Proc.*, **1988**, 86, 249.

Ong, V.S.; Hites, R.A. *J. Am. Soc. Mass Spectrom.*, **1993**, 4,270.

Pocsfalvi G.; Liptak, M.; Huszthy, P.; Bradshaw, J.; Izatt, R.M.; Vekey, K. *Anal. Chem.*, **1996**, 68, 792.

Quarmby, S.T. Ph.D. Dissertation, University of Florida, Gainesville, FL, **1997**.

Rankin, P.C. *J. Assoc. Offic. Anal. Chem.*, **1971**, 54, 1340.

Sawada, M.; Okumura, Y.; Yamada, H.; Takai, Y.; Takahashi, S.; Kaneda, T.; Hirose, K.; Misumi, S. *Org. Mass Spectrom.*, **1993**, 28, 1525.

Sears, L.J.; Grimsrud, E.P. *Anal. Chem.*, **1989**, 61, 2523.

Sellier, N.M.; Bouillet, C.T.; Douay, D.L.; and Tabet, J.E. *Rapid Comm. Mass Spectrom.*, **1994**, 8, 892.

Solomons, T.G. *Organic Chemistry,* 4th ed., John Wiley and Sons, New York, **1988**, pp. 470-471.

Soni, M.; Amy, J.; Frankevich, V.; Cooks, R.G.; Taylor, D.; McKewan, A.; Schwartz, J.C. *Rapid Comm. Mass Spectrom.*, **1995**, 9, 911.

Splitter, J.S.; Turecek, F. *Applications of mass Spectrometry to Organic Stereochemistry*, VCH, New York, **1994**.

Stafford, G.C.; Kelly, P.E.; Stephens, D.R. United States Patent 4,540,884, **1985**.

Stein, S.; Levitsky, A.; Fateev, O.; Mallard, G. The NIST Mass Spectral Search Program for the NIST/EPA/NIH Mass Spectral Library, ver. 1.6, NIST, Gaithersburg, MD, 1997.

Stemmler, E.A.; Hites, R.A. *Electron Capture Negative Ion Mass Spectra of Environmental Contaminants and Related Compounds*, VCH, Weinham, **1988**.

Thompson, M.Q. Chapter 2: Pressure/Flow Relationships in Capillary Gas Chromatography, In Stafford, S.S. (Ed.) *Electronic Pressure Control in Gas Chromatography,* 2nd ed., Hewlett-Packard Co., Wilmington, DE, **1994**.

Vekey, K.; Czira, G. *Anal. Chem.*, **1997**, 69, 1700.

Warman, J.M.; Sauer, M.C., Jr. *J. Chem. Phys.* **1975**, 62, 1971.Winkler, F.J.; Medina, R.;

Winkler, J.; Krause, H. *J. Chromatogr. A*, **1994**, 666, 549.

Yates, N.A.; Yost, R.A.; Bradshaw, S.C.; Tucker, D.B. *Proc. of the 39th ASMS Conf. Mass Spectrom. and Allied Topics*, Nashville, TN, **1991**, p.1489.

Yost, R.A.; Pedder, R.E. *Proc. of the 37th ASMS Conf. Mass Spectrom. and Allied Topics*, Miami Beach, FL, **1989**, p.62

BIOGRAPHICAL SKETCH

George Brody Guckenberger, V, was born on March 27, 1971, in Bryan, Ohio. He lived in Hamilton, Indiana, through the second grade and then moved to Wyoming, Ohio, in 1979. As a youth, Brody was active in Boy Scouts, Science Olympiad, Cincinnati Junior Strings, wrestling, football, and track. In 1989 he graduated from Wyoming High School.

Brody continued his education at Vanderbilt University, where he was active in Reformed University Fellowship, track, orchestra, and Lambda Chi Alpha fraternity. Majoring in chemistry, Brody worked for Dr. Lynmarie A. Posey over the summers of 1992 and 1993, helping to build a novel mass spectrometer for spectroscopic study of gas-phased ion clusters. For his undergraduate research, he was awarded the Stephen Harris Cook Fellowship and Donald E. Pearson Award. In May of 1993 he received his BA in chemistry from Vanderbilt University.

In the fall of 1993, Brody began his graduate studies in physical chemistry at the University of Florida. On June 3, 1995, Brody married Alison Lynn Brown in Savannah, Georgia. Brody spent the summers of 1997 and 1998 as an intern scientist with Finnigan in Austin, Texas. He remained at the University of Florida under the direction of Dr. Richard A. Yost for the completion his PhD.

I certify that I have read this study and that in my opinion it conforms to acceptable standards of scholarly presentation and is fully adequate, in scope and quality, as a dissertation for the degree of Doctor of Philosophy.

Richard A. Yost, Chairman
Professor of Chemistry

I certify that I have read this study and that in my opinion it conforms to acceptable standards of scholarly presentation and is fully adequate, in scope and quality, as a dissertation for the degree of Doctor of Philosophy.

Christopher D. Batich
Professor of Materials Science and Engineering

I certify that I have read this study and that in my opinion it conforms to acceptable standards of scholarly presentation and is fully adequate, in scope and quality, as a dissertation for the degree of Doctor of Philosophy.

John R. Eyler
Professor of Chemistry

I certify that I have read this study and that in my opinion it conforms to acceptable standards of scholarly presentation and is fully adequate, in scope and quality, as a dissertation for the degree of Doctor of Philosophy.

Luis M. Muga
Professor of Chemistry

I certify that I have read this study and that in my opinion it conforms to acceptable standards of scholarly presentation and is fully adequate, in scope and quality, as a dissertation for the degree of Doctor of Philosophy.

William Weltner
Professor of Chemistry

This dissertation was submitted to the Graduate Faculty of the Department of Chemistry in the College of Liberal Arts and Sciences and to the Graduate School and was accepted as partial fulfillment of the requirements for the degree of Doctor of Philosophy.

May 1999

_____

Dean, Graduate School